THE ASTROPHYSICAL JOURNAL, 473:88–109, 1996 December 10

A PRECISE DISTANCE INDICATOR: TYPE Ia SUPERNOVA MULTICOLOR LIGHT-CURVE SHAPES

ADAM G. RIESS, WILLIAM H. PRESS, AND ROBERT P. KIRSHNER
Harvard-Smithsonian Center for Astrophysics, 60 Garden Street, Cambridge, MA 02138
Received 1996 April 15; accepted 1996 June 21

ABSTRACT

We present an empirical method that uses multicolor light-curve shapes (MLCSs) to estimate the luminosity, distance, and total line-of-sight extinction of Type Ia supernovae (SNe Ia). The empirical correlation between the MLCSs and the luminosity is derived from a "training set" of nine SN Ia light curves with independent distance and reddening estimates. We find that intrinsically dim SN Ia's are redder and have faster light curves than the bright ones, which are slow and blue. By 35 days after maximum, the intrinsic color variations become negligible. A formal treatment of extinction employing Bayes's theorem is used to estimate the best value and its uncertainty. Applying the MLCS method to both light curves and to color curves provides enough information to determine which supernovae are dim because they are distant, which are intrinsically dim, and which are dim because of extinction by dust. The precision of the MLCS distances is examined by constructing a Hubble diagram with an independent set of 20 SN Ia's. The dispersion of 0.12 mag indicates a typical distance accuracy of 5% for a single object, and the intercept yields a Hubble constant on the Sandage et al. Cepheid distance scale of $H_0 = 64 \pm 3$ (statistical) km s^{-1} Mpc^{-1} (± 6 total error). The slope of 0.2010 ± 0.0035 mag over the distance interval $32.2 < \mu < 38.3$ yields the most precise confirmation of the linearity of the Hubble law.

Subject headings: distance scale — dust, extinction — supernovae: general

1. INHOMOGENEITY OF TYPE Ia SUPERNOVAE

Since the Curtis-Shapley debate of 1920 (Curtis 1921; Shapley 1921), the determination of supernova (SN) luminosities has been central to the discussion of extragalactic distances. Shapley (1921) argued against the "Island Universe" hypothesis because it required certain novae (such as S Andromedae of 1885) to reach the astonishing luminosity of $M = -16$. He considered this to be "out of the question." Curtis (1921) countered, concluding that "the dispersion of the novae in spirals and in our galaxy may reach ten absolute magnitudes ... a division into two classes is not impossible." This distinction between novae and supernovae, required by the extragalactic nature of the nebulae, was later made explicit by Baade & Zwicky (1934). They showed that in addition to their tremendous difference in absolute luminosity, the photometric and spectroscopic behavior of supernovae is distinct from novae. Baade (1938) showed that supernovae were more uniform than novae, with a dispersion at peak of 1.1 mag, making them suitable as extragalactic distance indicators.

The precision of supernova distance estimates has increased as the SN Ia class has been better understood and more narrowly defined. The low dispersion in Baade's sample benefited from the fortuitous absence of Type II supernovae, which are significantly less luminous in the mean. Beginning with SN 1940B, Type II supernovae were classified by the presence of hydrogen in their spectra (Minkowski 1941). The growing list of spectroscopically defined Type I supernovae had dispersions at peak of 0.8–0.6 mag (Minkowski 1964; Kowal 1968; Kirshner et al. 1973; Oke & Searle 1974). However, this sample included a number of "peculiar" SN I noted for their lack of silicon, which are now recognized to arise from massive stars that lose their envelope before core collapse (see Wheeler & Harkness 1990). After removing these silicon-deficient objects, now classified as Ib's and Ic's (Doggett & Branch 1985; Uomoto & Kirshner 1985; Wheeler & Levreault 1985; Wheeler & Harkness 1990), the remaining Type Ia supernovae (SN Ia's) form a more homogeneous set that serves as an even more precise indicator of astronomical distances. Leibundgut (1989) devised a set of standard templates to describe the photometric behavior of SN Ia's and to estimate the peak apparent magnitude. Hubble diagrams constructed using the peak of photographic SN Ia light curves had observed dispersions ranging from $\sigma_M = 0.65$–0.36 mag depending on which objects and color bands were used (Tammann & Leibundgut 1990; Branch & Miller 1993; Miller & Branch 1990; Della Valle & Panagia 1992; Rood 1994; Sandage & Tammann 1993; Sandage et al. 1992, 1994). An ambitious program to calibrate nearby SN Ia's through Cepheid variables observed with the *Hubble Space Telescope* has been undertaken by Sandage et al. (1992, 1994, 1996). Assuming SN Ia's to be homogeneous yields a Hubble constant in the range 50–58 km s^{-1} Mpc^{-1} (Sandage et al. 1992, 1994, 1996; Schaefer 1994, 1995a, 1995b, 1996; Branch & Tammann 1992) with the most recent measurement giving 57 ± 4 km s^{-1} Mpc^{-1}. We show in §§ 6 and 7 that the precision of this measurement is improved and the value of H_0 is altered by including information contained in the light and color curve shapes.

The hypothesis that SN Ia's are standard candles drew support not only from empirical studies, but also from the earliest theoretical models, which suggested that they arose from ignition of a carbon-oxygen white dwarf at the Chandrasekhar mass (Hoyle & Fowler 1960; Arnett 1969; Colgate & McKee 1969). In these models, a supersonic shock wave travels through the degenerate star, burning material into ^{56}Ni at a temperature of 5×10^9 degrees (Khokhlov, Müller, & Höflich 1993; Mazurek & Wheeler 1980). Because the detonation is supersonic, the preshock region cannot expand to decrease the pressure or the burning temperature. Furthermore, the Fermi pressure of the degenerate material in the postshock region remains insensitive to temperature for longer than the burning timescale. The result is a total incineration and the production of a pure mass of

nickel. Such a standard explosion of a uniform mass would lead to a homogeneous light curve and uniform luminosity. Yet, these complete burning models of Ia's do not reproduce the intermediate-mass elements that are seen in the spectra of SN Ia's (Wheeler & Harkness 1990). A successful model (Nomoto, Thielemann, & Yokoi 1984) that matched the observational constraints was so persuasive that Arnett, Branch, & Wheeler (1985) and Branch (1992) suggested calibration of the Hubble constant based only on theoretical models of uniform nickel production. However, a variety of models (Livne 1990; Khokhlov et al. 1993; Woosley & Weaver 1994; Höflich, Khokhlov, & Wheeler 1995) match the observed features of the spectra and produce a range of nickel masses and a range of predicted luminosities. These models employ subsonic deflagration fronts, pulsations, or off-center explosions to allow the surface layers to preexpand and burn at low temperature. The success of these models in reproducing the observed spectra opens a large range of theoretical possibilities. Unlike the first monoenergetic models, these models suggest that a wide range of luminosities might result from the ignition of a white dwarf.

Recently, precise observations of SN Ia's made with CCD detectors show evidence for inhomogeneity in both luminosity and light-curve shape. One of the first SN Ia's observed with a distinctly different light curve was 1986G (Phillips et al. 1987; Cristiani et al. 1992), which displayed a spectacularly rapid decline in its B and V light curve and unique spectral characteristics including stronger than usual Si features. Although SN 1986G was heavily reddened by dust, reddening cannot alter significantly the *shape* of the light curve. SN 1991bg in NGC 4374 is the most extreme SN Ia in an increasingly apparent photometric and spectral sequence. Leibundgut et al. (1993) (also Filippenko et al. 1992) described a number of photometric abnormalities of 1991bg with respect to his templates. These include the fastest postmaximum decline (2.05 and 1.42 mag decrease drop in B and V in the 15 days after maximum compared to 1.22 and 0.64 mag for the templates in B and V), a narrow luminosity peak, and an intrinsic red color near maximum. A simple and convincing argument that SN Ia's have a large spread in luminosity is that SN 1957B, which occurred in the same galaxy, was 2.5 mag brighter in B than SN 1991bg. In addition, SN 1991bg was at least 2 mag fainter than other SN Ia's in the Virgo Cluster, of which NGC 4374 is a member. This extreme SN Ia seems to have a twin in the subluminous SN 1992K (Hamuy et al. 1994), which strongly resembles 1991bg in photometric and spectral behavior.

At the opposite extreme of the SN Ia class, SN 1991T showed spectral and photometric peculiarities that were different from those seen in the rapid decliners. Phillips et al. (1992) found the light curves in B and V to rise and decline more slowly than the standard templates near maximum, and a month after peak, this shallower decline resulted in a light curve 0.2–0.3 mag brighter than the templates. Although SN 1991T's host galaxy, NGC 4527, appears to lie south of the main Virgo Cluster, Phillips et al. (1992) estimates that the peak luminosity exceeded that of other SN Ia's in Virgo by 0.3–0.5 mag. From the narrow Na I D absorption line, Filippenko et al. (1992) deduced that SN 1991T is dimmed by dust in NGC 4527 and concluded that it may have been as much as ~ 0.9 mag more luminous than a typical SN Ia. More recently, the Calán/CTIO supernova search yielded SN 1992bc and 1992bo (Maza et al. 1994), two SN Ia's with similar recession velocities of 6050 and 5660 km s^{-1}, but with peak apparent luminosities differing by 0.69 mag in B. The large difference in apparent magnitude and the small difference in recession velocity imply that SN 1992bc was intrinsically brighter by 0.8 ± 0.2 mag than 1992bo. For a difference in distance to account for this difference in luminosity, the peculiar velocities of the two supernovae would have to differ by ~ 2500 km s^{-1}, an unlikely alternative. Interestingly, SN 1992bc declined more slowly than the average template, while SN 1992bo's postmaximum fall was more rapid than the average template, a result in good accord with later analysis by Phillips (1993).

Even before these recent examples of inhomogeneity, less precise photographic measurements by Barbon, Ciatti, & Rosino (1973) suggested that there might exist two photometric classes: those which "fast" decline rates after maximum, which were intrinsically brighter supernovae, and those with "slow" decline rates, which were fainter. With the poor quality of photographic and photoelectric photometry then available, such a real distinction was difficult to demonstrate convincingly. Pskovskii (1977, 1984) suggested a continuous photometric sequence of SN Ia light curves. He introduced a parameter, β: the slope of the B-band postmaximum decline in magnitudes per 100 days. Using 54 photographic SN Ia light curves, Pskovskii found a weak correlation between β and the absolute B magnitude at maximum light that was *opposite* to that of Barbon et al. (1973). Early difficulties in measuring a relation between SN Ia light-curve shape and intrinsic luminosity resulted from noisy photographic data that were poorly sampled and calibrated. These difficulties were compounded by the problem of measuring a decaying light curve on a bright galaxy with a nonlinear photographic detector (Boisseau & Wheeler 1991). With the advantage of better data measured with linear detectors, Phillips (1993) demonstrated conclusive evidence for a luminosity–light curve decline relation among SN Ia. Using a set of well-sampled SN Ia light curves with precise optical photometry and accurate relative distances, Phillips found that the absolute luminosity in B, V, and I is correlated with the B-band decline in the 15 days following maximum light. The sense of the correlation is that dimmer SN Ia's fall more rapidly after maximum than bright SN Ia's. Application of this relation to his sample results in a significant reduction of the dispersion in B, V, and I luminosity from 0.8, 0.6, and 0.5 mag to 0.36, 0.28, and 0.38 mag, respectively. A more recent investigation by Tammann & Sandage (1995) has examined the luminosity–light curve decline relation among "normal" SN Ia's; in this case "normal" is defined as having a $(B-V)_{\max} \leq 0.30$ mag. They tentatively confirm a luminosity dependence on light-curve decline, with a slope that is shallower than Phillips (1993) but consistent with Hamuy et al. (1995) for a similar set of "normal" SN Ia's. In § 6 we show for a sample restricted to "normal" SN Ia's, a significant correlation between light-curve shape and luminosity exists.

This empirical relation between light curves and luminosity in SN Ia's has been paced by an abundance of theoretical models that can account for the observed behavior (Höflich, Müller, & Khokhlov 1993; Woosley & Weaver 1994; Ruiz-Lapuente et al. 1993; Livne & Arnett 1995; Höflich & Khokhlov 1996). These new models include deflagration burning fronts, off-center detonations, surface helium burning, pulsed delayed detonations, and sub-Chandrasekhar progenitors. These models give plausible causes for the observed inhomogeneity of SN Ia's and for the origin of the empirical relations between light-curve shape and luminosity.

Most recently, Hamuy et al. (1995) have employed a template-fitting approach, and we (Riess, Press, & Kirshner 1995a, hereafter RPK95a) have developed a linear estimation algorithm to use the distance-independent light-curve shapes to improve the precision of distance measurements to SN Ia's. The techniques have much in common, and both yield Hubble diagram dispersions of ~ 0.2 mag for an overlapping set of objects. The light curve shape (LCS) method, described in RPK95a, has the advantage of providing quantitative error estimates for the distance. The present paper extends the LCS technique to use the shapes of $B-V$, $V-R$, and $V-I$ color curves, which provide enough information to determine the relation between absolute luminosity and intrinsic color. Knowledge of an SN Ia's intrinsic color allows us to measure the extinction from the observed reddening. For each well-observed SN Ia we measure the luminosity, the extinction, and the extinction-corrected distance. The multicolor light-curve shape (MLCS) method increases significantly the precision of distance estimates from SN Ia light curves, as we show in § 6.

There are many potential applications for a bright distance indicator with $<10\%$ precision. Nearby ($0.01 \leq z \leq 0.1$), it should be possible to measure the Hubble constant to an accuracy that is limited only by the underlying calibration of Cepheids. It is important to compare the Hubble constant derived using the light-curve shape-luminosity relation with determinations that have assumed a homogeneous luminosity for SN Ia's (Sandage et al. 1994, 1996). Using the velocity residuals from Hubble flow, we have measured the motion of the Local Group with respect to the rest frame of galaxies with supernovae (Riess, Press, & Kirshner 1995b). At even greater distances ($0.3 \leq z \leq 0.6$), MLCS distance measurements of all well-observed SN Ia's could be used to determine the cosmological deceleration parameter, q_o (Perlmutter et al. 1995, 1996; Schmidt et al. 1996; IAU Circ. 6160).

Some have sought to improve the homogeneity of the observed SN Ia's by restricting the sample to supernovae with "normal" spectra (Branch, Fisher, & Nugent 1993; Sandage et al. 1994, 1996). While spectroscopic information may prove useful in producing smaller dispersion in distance estimates, the difficulty in obtaining good spectra of very distant SN Ia's makes it hard to identify subtle spectral variations. A sample cut that cannot be applied with equal effectiveness for nearby and for distant SN Ia's could lead to a bias in cosmological parameters determined by them. We prefer to develop a method that can be applied to all SN Ia's.

Given at least one light curve and one color curve, observed photoelectrically within 10 days after maximum, our MLCS method can distinguish between the effects of distance, intrinsic dimness, and dust for all SN Ia's. In §§ 2–5 we develop the multicolor light-curve shape method for measuring extinction-corrected distances. In § 6, for an independent sample, we compare the extinction-corrected MLCS distances with distances determined by more limited assumptions. In § 7, we estimate the Hubble constant and discuss sample membership, selection bias, and the range of progenitors that may be responsible for the empirical range of SN Ia luminosities and colors.

2. LEARNING CURVES

SN Ia light curves are noisy unevenly sampled time series, which, when observed diligently, are available in four bands, B, V, R, and I. Although some SN Ia's are found in ellipticals, most are found in spirals and irregulars, where they can be subject to significant extinction by dust. At present, the number of well-sampled SN Ia light curves available on a modern photometric system is limited (i.e., ≤ 50) (Hamuy et al. 1995; Riess et al. 1996a; Ford et al. 1993; Richmond et al. 1995).

We employ a general χ^2 model to establish the empirical relation between light and color curve shape and luminosity from a nearby subset of SN Ia's with accurately known *relative distances* and extinctions. Then we use these results to estimate the extinction-corrected distance for a separate distant sample *solely from the observed light and color curves.* The observables are a visual band light curve and up to three color curves.

To first approximation, the observed light and color curves of SN Ia's are homogeneous, resembling standard template light and color curves with the addition of noise ($\boldsymbol{n}$) for each color and individual offsets that result from the apparent visual distance modulus (μ_V) and a color excess ($E_{\rm color}$) due to reddening by dust:

$$\boldsymbol{m_V} = \boldsymbol{M_V} + \mu_V + \boldsymbol{n_V}\,, \tag{1}$$

$$\boldsymbol{m_B} - \boldsymbol{m_V} = (\boldsymbol{B-V})_0 + E_{B-V} + \boldsymbol{n_{B-V}}\,, \tag{2}$$

$$\boldsymbol{m_V} - \boldsymbol{m_R} = (\boldsymbol{V-R})_0 + E_{V-R} + \boldsymbol{n_{V-R}}\,, \tag{3}$$

$$\boldsymbol{m_V} - \boldsymbol{m_I} = (\boldsymbol{V-I})_0 + E_{V-I} + \boldsymbol{n_{V-I}}\,, \tag{4}$$

Here bold-face type denotes a vector whose entries are measured or determined as a function of time. In standard convention, M is an absolute magnitude, m is an apparent magnitude, and $(B-V)_0$, $(V-R)_0$, and $(V-I)_0$ are unreddened color curves. Each available color curve yields an $E_{\rm color}$ term which, combined with a standard extinction curve, reduces the uncertainty in measuring the total line-or-sight extinction, A_V. This description of light and color curves assumes intrinsic homogeneity of SN Ia's, and is equivalent to the "template" approach of Leibundgut (1989), Sandage et al. (1994, 1996), and Sandage & Tammann (1993).

Improvements in the quality of the available data set and the success of Phillips (1993) motivate an approach which, to first order, can account for the observed variations in the light and color curves and intrinsic luminosity. The most economical approach is to adopt a single parameter and correlate it with the variations of the observed curves. The natural parameter to choose is the amount by which the intrinsic luminosity differs from an SN Ia of standard brightness and curve shape since, in the end, it is this difference we hope to measure. We call this the "luminosity correction," Δ, where $\Delta \equiv M_V - M_{V,\rm standard}$, and $M_{V,\rm standard}$ is the luminosity of the SN Ia chosen to depict the "standard" SN Ia event. This difference is measured by convention at the date of B maximum. The functions of time which, to first order in Δ, correct the observed curves to the template curves are "correction templates," $R_V(t)$ or $R_{\rm color}(t)$. Using these definitions, we expect two supernovae whose

absolute visual luminosities differ by Δ magnitudes to have light and color curves that differ by $R_V(t)\Delta$ and $R_{\rm color}(t)\Delta$. The assumption that luminosity correlates *linearly* with light and color curve shape need not provide a complete description, but given the limitations of our real data sets, it is a reasonable way to begin. The evidence that this is a useful way to proceed is provided in § 6, where we show that this method produces a significant decrease in the dispersion for an independent set of SN Ia's in the Hubble flow.

Our improved model for the light and color curves is thus

$$\boldsymbol{m_V} = \boldsymbol{M_V} + \mu_V + \boldsymbol{R_V}\Delta + \boldsymbol{n_V}\,, \tag{5}$$

where $R_V(t)\Delta$ gives the deviation from the template, $M_V(t)$, at each time. Similarly,

$$\boldsymbol{m_B} - \boldsymbol{m_V} = (\boldsymbol{B}-\boldsymbol{V})_0 + E_{B-V} + \boldsymbol{R_{B-V}}\Delta + \boldsymbol{n_{B-V}}\,, \tag{6}$$

$$\boldsymbol{m_V} - \boldsymbol{m_R} = (\boldsymbol{V}-\boldsymbol{R})_0 + E_{V-R} + \boldsymbol{R_{V-R}}\Delta + \boldsymbol{n_{V-R}}\,, \tag{7}$$

$$\boldsymbol{m_V} - \boldsymbol{m_I} = (\boldsymbol{V}-\boldsymbol{I})_0 + E_{V-I} + \boldsymbol{R_{V-I}}\Delta + \boldsymbol{n_{V-I}}\,, \tag{8}$$

where $(B-V)_0$, $(V-R)_0$, and $(V-I)_0$ are the unreddened template color curves. It is instructive to compare equations (5)–(8), which allow SN Ia inhomogeneity, to equations (1)–(4), which impose SN Ia homogeneity.

In matrix format, we can write equations (5)–(8) as one system of equations,

$$\begin{pmatrix} m_V(t_1) \\ m_V(t_2) \\ \cdot \\ m_V(t_N) \\ m_B(t_1) - m_V(t_1) \\ m_B(t_2) - m_V(t_2) \\ \cdot \\ m_B(t_N) - m_V(t_N) \\ m_V(t_1) - m_R(t_1) \\ m_V(t_2) - m_R(t_2) \\ \cdot \\ m_V(t_N) - m_R(t_N) \\ m_V(t_1) - m_I(t_1) \\ m_V(t_2) - m_I(t_2) \\ \cdot \\ m_V(t_N) - m_I(t_N) \end{pmatrix} = \begin{pmatrix} M_V(t_1) \\ M_V(t_2) \\ \cdot \\ M_V(t_N) \\ (B-V)_0(t_1) \\ (B-V)_0(t_2) \\ \cdot \\ (B-V)_0(t_N) \\ (V-R)_0(t_1) \\ (V-R)_0(t_2) \\ \cdot \\ (V-R)_0(t_N) \\ (V-I)_0(t_1) \\ (V-I)_0(t_2) \\ \cdot \\ (V-I)_0(t_N) \end{pmatrix} + \begin{pmatrix} 1 & 0 & R_V(t_1) \\ 1 & 0 & R_V(t_2) \\ \cdot & \cdot & \cdot \\ 1 & 0 & R_V(t_N) \\ 0 & \frac{1}{3.1} & R_{B-V}(t_1) \\ 0 & \frac{1}{3.1} & R_{B-V}(t_2) \\ \cdot & \cdot & \cdot \\ 0 & \frac{1}{3.1} & R_{B-V}(t_N) \\ 0 & \frac{1}{3.9} & R_{V-R}(t_1) \\ 0 & \frac{1}{3.9} & R_{V-R}(t_2) \\ \cdot & \cdot & \cdot \\ 0 & \frac{1}{3.9} & R_{V-R}(t_N) \\ 0 & \frac{1}{1.9} & R_{V-I}(t_1) \\ 0 & \frac{1}{1.9} & R_{V-I}(t_2) \\ \cdot & \cdot & \cdot \\ 0 & \frac{1}{1.9} & R_{V-I}(t_N) \end{pmatrix} \times \begin{pmatrix} \mu_V \\ A_V \\ \Delta \end{pmatrix} + n(t)\,, \tag{9}$$

where we have combined the $E_{\rm color}$ terms into one simultaneous measurement of A_V with the aid of the standard reddening law parameterization, $A_V/[E(B-V)] = 3.1$, $A_V/[E(V-R)] = 3.9$, $A_V/[E(V-I)] = 1.9$ (Savage & Mathis 1979). Here we assume the Galactic reddening ratios are valid for the dust in distant galaxies. Elsewhere, we examine the homogeneity of these ratios in distant galaxies, and we find that the most likely form of the reddening law for dust in distant galaxies is consistent with the Galactic reddening law (Riess, Press, & Kirshner 1996b).

The χ^2 of the fit between data and model is

$$\chi^2 = (\boldsymbol{n})^T \boldsymbol{C}^{-1}(\boldsymbol{n})\,, \tag{10}$$

where $\boldsymbol{n}$ is the vector of residuals in equations (5)–(8) or equivalently in equation (9). Here $\boldsymbol{C}$ is the correlation matrix whose elements are intended to reflect the errors in observations and residual, unmodeled correlations in SN Ia light and color curves. The correlation matrix is discussed in detail in § 4.

Rybicki & Press (1992) have derived two analytical minimizations of the χ^2 given in equation (10). One gives the best estimate of the correction templates, $R_V(t)$ or $R_{\rm color}(t)$, provided the SN Ia parameters, $[\mu_V, A_V, \Delta]$, are known, and the other gives the best estimate of the parameters, provided the correction templates are known. We employ both, using the nearby set with accurate relative distances as a "training set" to estimate $R_V(t)$ and $R_{\rm color}(t)$. Once trained, we measure the μ_V, A_V, and Δ parameters for an independent set of SN Ia's from the shapes of their light and color curves.

Analytical minimization of χ^2 in equation (10) with respect to $R_V(t)$ or $R_{\rm color}(t)$ is independent of $\boldsymbol{C}$ and gives

$$R_V(t) = \frac{\langle [m_V(t) - M_V(t) - \mu]\Delta \rangle}{\langle \Delta^2 \rangle}, \tag{11}$$

or

$$R_{\rm color}(t) = \frac{\langle [m_{\rm color}(t) - M_{\rm color}(t) - E_{\rm color}]\Delta \rangle}{\langle \Delta^2 \rangle}, \tag{12}$$

where the angle brackets denote an average over the training set weighted by the uncertainty in the given estimates of Δ.

It is convenient to choose a particular object as the "standard" SN Ia whose light and color curves define the standard template curves, $M_V(t)$ and $M_{\rm color}(t)$. By definition, the "standard" SN Ia's have a peak luminosity variation of $\Delta \equiv 0$. The utility of the method is insensitive to the choice of the template curves and luminosity, since all quantities are defined relative to it. Leibundgut's templates, made from SN 1989B, SN 1980N, and SN 1981B, approximate the light curves of the "normal" training set supernovae in B and V. For R and I, we have constructed our own templates from SN 1989B, SN 1980N, and SN 1981B.

In solving for the correction templates, we only need consistent *relative* distances for our training set of SN Ia's, since we correlate luminosity *differences* with light-curve shape variation. No choice of absolute distance scale is necessary because all luminosity corrections, Δ, are relative to the standard SN Ia. Surface brightness fluctuations (SBFs), planetary nebula luminosity function (PNLF), and Tully and Fisher's luminosity–line width relation (T-F) provide accurate and consistent bias-corrected *relative* distances to the host galaxies of the training set of SN Ia's (Strauss & Willick 1995; Jacoby et al. 1992; Ciardullo, Jacoby, & Tonry 1993; Pierce 1994; Kennicutt, Freedman, & Mould 1995). We have no dogma about the correctness of this *absolute* distance scale—in § 7 we calibrate the absolute luminosity of a standard SN Ia, contained in $M_V(t)$ with the Cepheid observations from Sandage et al. (1994, 1996). This approach has the advantage of placing our distance scale directly onto that of the Cepheid variables. Published SBF distances have been undergoing some modifications (J. Tonry, private communication). We comment on the effect of changes in SBF distances in § 7.

The training set of supernovae we have used also has precise optical photometry, well-sampled light curves, and estimates of $E(B-V)$ (see Table 1). The color excesses in Table 1 are estimated from comparisons with unreddened, photometrically similar SN Ia's (Phillips 1993; Wells et al. 1994) and are used to correct the luminosity and color curves of the affected objects. In § 7 we discuss our training set membership. On the SBF-PNLF-TF distance scale, SN Ia's that define the template have an $\langle M_V \rangle = -18.54$ on the date of B maximum; therefore, each supernova's $\Delta \equiv M_V - (-18.54)$. We have calculated the correction templates from equations (11) and (12) using the training set of supernovae provided in Table 1. The correction templates and standard templates are listed in Table 2. The standard template, $M_V(t)$, as listed in Table 2, is calibrated on the Cepheid distance scale discussed in § 7.

Adding various amounts of the correction templates to the standard templates generates an empirical family of light and color curves (see Fig. 1). This family of curves demonstrates some interesting relations between light-curve behavior and luminosity. The natural history of SN Ia's is that intrinsically dim SN Ia's rise and fall rapidly in V as compared to the leisurely rise and fall of intrinsically bright SN Ia's. These results are similar to those of Phillips (1993) with the advantage that they show the SN Ia behavior from before maximum and more than 15 days after maximum.

An interesting new result is the quantitative relation between SN Ia luminosity and color. Supernova luminosities correlate with their intrinsic colors at early times (see also Lira 1995). Before day 35, the dim SN Ia's are red and the bright ones are

TABLE 1

TRAINING SET

SN	Galaxy	$\mu(\sigma)$	Method[a]	Reference	$E(B-V)(\sigma)$	M_V	$\Delta(\sigma)$	References
1980N	N1316	31.15(0.10)	SBF, PNLF	1	0.00(0.02)	−18.71	−0.17(0.10)	2
1981B.....	N4436	30.50(0.30)	T-F	3	0.00(0.02)	−18.54	0.00(0.32)	4
1986G	N5128	27.72(0.10)	SBF, PNLF	1	0.60(0.10)	−18.13	0.41(0.31)	5
1989B.....	N3627	29.40(0.30)	T-F	3	0.35(0.03)	−18.50	0.04(0.31)	6
1990N	N4639	31.40(0.30)	T-F	3	0.01(0.02)	−18.82	−0.28(0.31)	7
1991T.....	N4527	30.60(0.30)	T-F	3	0.00(0.02)	−19.10	−0.56(0.31)	8, 9
1991bg.....	N4374	31.05(0.10)	SBF, PNLF	1	0.00(0.02)	−17.10	1.44(0.10)	10, 11
1992A	N1380	30.65(0.11)	SBF	12	0.00(0.02)	−18.10	0.44(0.13)	13
1994ae	N3370	31.28(0.30)	T-F	14	0.14(0.03)	−18.65	−0.13(0.03)	15

[a] SBF = surface brightness fluctuations; PNLF = planetary nebula luminosity function; T-F = Tully-Fisher relation.

REFERENCES.—(1) Ciardullo et al. 1993. (2) Hamuy et al. 1991. (3) Pierce 1994. (4) Buta & Turner 1993. (5) Phillips et al. 1987. (6) Wells et al. 1994. (7) Leibundgut et al. 1991. (8) Phillips et al. 1992. (9) Ford et al. 1993. (10) Filippenko et al. 1992. (11) Leibundgut et al. 1993. (12) Tonry 1991. (13) Suntzeff et al. 1996. (14) Dell'Antonio 1995. (15) Riess et al. 1996a.

TABLE 2

TRAINING VECTORS

phase		standard templates				correction templates			weighting vectors			
t_{Bmax}	$M_V(t)$	$M_{B-V}(t)$	$M_{V-R}(t)$	$M_{V-I}(t)$	$R_V(t)$	$R_{B-V}(t)$	$R_{V-R}(t)$	$R_{V-I}(t)$	$\sigma_V(t)$	$\sigma_B(t)$	$\sigma_R(t)$	$\sigma_I(t)$
-11.000	-18.061	-0.307	0.007	0.390	1.257	0.492	0.273	0.408	0.000	0.371	0.130	0.251
-10.000	-18.374	-0.326	0.009	0.294	1.257	0.493	0.273	0.408	0.002	0.366	0.112	0.221
-9.000	-18.534	-0.285	0.012	0.260	1.257	0.493	0.273	0.408	0.008	0.349	0.112	0.216
-8.000	-18.693	-0.244	0.015	0.227	1.259	0.494	0.273	0.408	0.011	0.332	0.111	0.211
-7.000	-18.824	-0.216	0.019	0.185	1.259	0.491	0.272	0.404	0.013	0.316	0.114	0.212
-6.000	-18.955	-0.189	0.022	0.144	1.253	0.489	0.271	0.401	0.012	0.299	0.116	0.214
-5.000	-19.105	-0.102	0.029	0.002	1.249	0.479	0.268	0.407	0.011	0.284	0.119	0.219
-4.000	-19.183	-0.081	0.035	-0.079	1.244	0.474	0.257	0.408	0.010	0.270	0.123	0.226
-3.000	-19.246	-0.060	0.042	-0.157	1.220	0.473	0.257	0.412	0.008	0.258	0.125	0.233
-2.000	-19.296	-0.040	0.049	-0.216	1.160	0.471	0.257	0.412	0.007	0.248	0.128	0.241
-1.000	-19.334	-0.020	0.051	-0.267	1.093	0.468	0.258	0.412	0.006	0.239	0.130	0.249
0.000	-19.360	-0.000	0.046	-0.312	1.029	0.470	0.256	0.417	0.005	0.233	0.131	0.256
1.000	-19.375	0.021	0.034	-0.353	1.002	0.531	0.256	0.525	0.006	0.229	0.131	0.262
2.000	-19.380	0.043	0.014	-0.388	1.014	0.550	0.260	0.499	0.007	0.226	0.131	0.268
3.000	-19.375	0.068	-0.013	-0.418	1.033	0.576	0.256	0.615	0.008	0.226	0.130	0.273
4.000	-19.362	0.095	-0.042	-0.441	1.035	0.616	0.262	0.612	0.011	0.226	0.128	0.276
5.000	-19.340	0.125	-0.069	-0.458	1.060	0.668	0.291	0.658	0.014	0.228	0.126	0.279
6.000	-19.311	0.158	-0.091	-0.469	1.102	0.683	0.323	0.704	0.018	0.231	0.124	0.280
7.000	-19.275	0.194	-0.106	-0.473	1.142	0.734	0.372	0.747	0.022	0.235	0.121	0.280
8.000	-19.233	0.234	-0.115	-0.473	1.186	0.705	0.396	0.800	0.027	0.240	0.119	0.279
9.000	-19.187	0.277	-0.115	-0.468	1.233	0.675	0.418	0.851	0.033	0.245	0.116	0.277
10.000	-19.136	0.323	-0.109	-0.458	1.274	0.651	0.411	0.861	0.039	0.251	0.114	0.274
11.000	-19.082	0.372	-0.095	-0.443	1.317	0.629	0.406	0.870	0.045	0.256	0.111	0.270
12.000	-19.025	0.423	-0.075	-0.422	1.358	0.607	0.402	0.881	0.052	0.262	0.109	0.266
13.000	-18.967	0.476	-0.051	-0.394	1.396	0.583	0.397	0.893	0.058	0.267	0.107	0.261
14.000	-18.906	0.530	-0.022	-0.361	1.468	0.629	0.388	0.904	0.065	0.272	0.106	0.255
15.000	-18.845	0.584	0.010	-0.321	1.482	0.578	0.382	0.915	0.072	0.276	0.105	0.249
16.000	-18.783	0.638	0.044	-0.268	1.497	0.523	0.378	0.926	0.079	0.280	0.105	0.243
17.000	-18.721	0.692	0.078	-0.204	1.507	0.475	0.373	0.936	0.085	0.282	0.105	0.237
18.000	-18.660	0.745	0.112	-0.130	1.500	0.437	0.362	0.907	0.092	0.284	0.105	0.231
19.000	-18.598	0.796	0.146	-0.047	1.493	0.397	0.329	0.792	0.098	0.285	0.106	0.226
20.000	-18.537	0.844	0.177	0.043	1.487	0.352	0.294	0.690	0.104	0.285	0.107	0.220
21.000	-18.476	0.888	0.207	0.133	1.486	0.307	0.259	0.646	0.109	0.284	0.109	0.215
22.000	-18.415	0.930	0.233	0.220	1.493	0.270	0.226	0.601	0.115	0.282	0.111	0.211
23.000	-18.355	0.968	0.256	0.297	1.506	0.255	0.190	0.551	0.119	0.279	0.114	0.207
24.000	-18.295	1.002	0.276	0.365	1.488	0.207	0.159	0.502	0.124	0.275	0.116	0.204
25.000	-18.235	1.031	0.293	0.422	1.502	0.186	0.150	0.464	0.128	0.270	0.119	0.202
26.000	-18.176	1.056	0.306	0.469	1.479	0.166	0.140	0.426	0.131	0.264	0.123	0.200
27.000	-18.117	1.077	0.315	0.505	1.456	0.144	0.131	0.388	0.134	0.257	0.126	0.199
28.000	-18.059	1.094	0.321	0.537	1.439	0.122	0.122	0.350	0.137	0.250	0.129	0.199
29.000	-18.001	1.106	0.323	0.566	1.441	0.095	0.112	0.312	0.139	0.241	0.132	0.199
30.000	-17.944	1.114	0.323	0.591	1.439	0.076	0.103	0.273	0.141	0.233	0.136	0.200
31.000	-17.887	1.118	0.319	0.613	1.438	0.058	0.093	0.222	0.142	0.223	0.139	0.202
32.000	-17.832	1.119	0.315	0.631	1.436	0.040	0.084	0.158	0.144	0.214	0.142	0.205
33.000	-17.779	1.118	0.311	0.646	1.434	0.022	0.075	0.129	0.145	0.204	0.144	0.208
34.000	-17.726	1.113	0.307	0.657	1.431	0.005	0.066	0.109	0.145	0.193	0.147	0.211
35.000	-17.676	1.107	0.303	0.666	1.426	-0.011	0.061	0.094	0.145	0.183	0.149	0.215
36.000	-17.629	1.100	0.299	0.671	1.422	-0.026	0.064	0.090	0.146	0.173	0.150	0.219
37.000	-17.584	1.092	0.295	0.673	1.418	-0.041	0.067	0.086	0.145	0.163	0.152	0.223
38.000	-17.541	1.083	0.291	0.673	1.415	-0.052	0.070	0.081	0.145	0.153	0.153	0.228
39.000	-17.502	1.076	0.287	0.670	1.413	-0.049	0.073	0.076	0.145	0.144	0.153	0.232
40.000	-17.466	1.069	0.283	0.664	1.410	-0.047	0.075	0.072	0.145	0.135	0.154	0.237
41.000	-17.432	1.062	0.278	0.656	1.409	-0.045	0.077	0.069	0.144	0.127	0.153	0.241
42.000	-17.401	1.057	0.274	0.646	1.407	-0.042	0.078	0.067	0.144	0.119	0.153	0.245
43.000	-17.380	1.061	0.270	0.633	1.406	-0.040	0.080	0.065	0.143	0.112	0.152	0.249
44.000	-17.350	1.055	0.266	0.617	1.405	-0.038	0.081	0.063	0.143	0.106	0.151	0.252
45.000	-17.330	1.058	0.262	0.600	1.404	-0.035	0.083	0.060	0.143	0.100	0.149	0.255
46.000	-17.300	1.030	0.258	0.581	1.403	-0.033	0.084	0.058	0.142	0.095	0.148	0.257
47.000	-17.271	1.026	0.254	0.559	1.402	-0.031	0.086	0.062	0.142	0.091	0.146	0.258
48.000	-17.245	1.017	0.250	0.536	1.402	-0.031	0.091	0.134	0.142	0.088	0.143	0.259
49.000	-17.219	1.007	0.246	0.510	1.402	-0.031	0.097	0.165	0.143	0.086	0.141	0.259
50.000	-17.194	0.999	0.242	0.482	1.403	-0.028	0.099	0.198	0.143	0.084	0.139	0.258
51.000	-17.168	0.990	0.238	0.451	1.405	-0.035	0.103	0.224	0.143	0.084	0.136	0.257
52.000	-17.143	0.981	0.234	0.418	1.405	-0.028	0.107	0.138	0.144	0.084	0.134	0.254
53.000	-17.117	0.972	0.230	0.384	1.435	-0.042	0.108	0.194	0.145	0.085	0.132	0.251
54.000	-17.091	0.963	0.226	0.348	1.509	-0.069	0.109	0.252	0.146	0.087	0.130	0.247

TABLE 2—*Continued*

phase	standard templates				correction templates				weighting vectors			
t_{Bmax}	$M_V(t)$	$M_{B-V}(t)$	$M_{V-R}(t)$	$M_{V-I}(t)$	$R_V(t)$	$R_{B-V}(t)$	$R_{V-R}(t)$	$R_{V-I}(t)$	$\sigma_V(t)$	$\sigma_B(t)$	$\sigma_R(t)$	$\sigma_I(t)$
55.000	-17.066	0.955	0.222	0.311	1.485	-0.063	0.108	0.309	0.147	0.090	0.128	0.243
56.000	-17.040	0.945	0.218	0.273	1.493	-0.060	0.105	0.351	0.148	0.093	0.126	0.237
57.000	-17.015	0.937	0.213	0.236	1.495	-0.061	0.083	0.351	0.150	0.097	0.125	0.231
58.000	-16.989	0.928	0.209	0.199	1.488	-0.065	0.058	0.344	0.151	0.101	0.124	0.224
59.000	-16.963	0.918	0.205	0.162	1.487	-0.079	0.039	0.356	0.153	0.105	0.124	0.217
60.000	-16.938	0.910	0.201	0.125	1.496	-0.080	0.033	0.411	0.155	0.110	0.124	0.210
61.000	-16.912	0.901	0.197	0.088	1.504	-0.081	0.027	0.466	0.157	0.115	0.124	0.202
62.000	-16.887	0.892	0.193	0.051	1.515	-0.081	0.022	0.494	0.159	0.120	0.125	0.194
63.000	-16.861	0.883	0.189	0.013	1.525	-0.081	0.022	0.452	0.161	0.125	0.126	0.186
64.000	-16.835	0.874	0.185	-0.024	1.536	-0.081	0.022	0.425	0.163	0.130	0.128	0.178
65.000	-16.810	0.865	0.181	-0.061	1.547	-0.081	0.022	0.436	0.165	0.135	0.130	0.171
66.000	-16.784	0.856	0.177	-0.095	1.559	-0.082	0.022	0.447	0.167	0.140	0.133	0.163
67.000	-16.759	0.848	0.173	-0.127	1.571	-0.083	0.022	0.458	0.169	0.144	0.137	0.156
68.000	-16.733	0.839	0.169	-0.156	1.582	-0.084	0.022	0.470	0.171	0.148	0.140	0.150
69.000	-16.707	0.829	0.165	-0.182	1.594	-0.085	0.022	0.481	0.172	0.151	0.145	0.145
70.000	-16.682	0.821	0.161	-0.206	1.591	-0.084	0.022	0.493	0.174	0.153	0.149	0.140
71.000	-16.656	0.812	0.157	-0.226	1.552	-0.077	0.022	0.504	0.176	0.155	0.154	0.136
72.000	-16.631	0.803	0.153	-0.244	1.514	-0.070	0.022	0.516	0.177	0.156	0.160	0.133
73.000	-16.605	0.794	0.149	-0.262	1.491	-0.067	0.021	0.526	0.179	0.157	0.165	0.131
74.000	-16.579	0.785	0.144	-0.280	1.528	-0.079	0.021	0.536	0.180	0.156	0.171	0.130
75.000	-16.554	0.776	0.140	-0.298	1.558	-0.086	0.020	0.556	0.181	0.154	0.177	0.131
76.000	-16.528	0.767	0.136	-0.316	1.569	-0.081	0.020	0.588	0.182	0.152	0.183	0.133
77.000	-16.503	0.759	0.132	-0.334	1.580	-0.076	0.019	0.588	0.183	0.149	0.189	0.135
78.000	-16.477	0.750	0.128	-0.352	1.591	-0.071	0.019	0.589	0.184	0.144	0.195	0.139
79.000	-16.451	0.740	0.124	-0.370	1.602	-0.065	0.018	0.589	0.185	0.139	0.200	0.144
80.000	-16.426	0.732	0.120	-0.388	1.616	-0.060	0.018	0.588	0.185	0.133	0.206	0.150
81.000	-16.400	0.723	0.116	-0.406	1.626	-0.054	0.017	0.590	0.185	0.126	0.211	0.157
82.000	-16.375	0.714	0.112	-0.424	1.637	-0.048	0.017	0.591	0.185	0.119	0.216	0.165
83.000	-16.349	0.705	0.108	-0.442	1.648	-0.042	0.017	0.593	0.186	0.111	0.220	0.173
84.000	-16.323	0.696	0.104	-0.460	1.650	-0.036	0.017	0.595	0.186	0.102	0.224	0.182
85.000	-16.298	0.688	0.100	-0.478	1.615	-0.035	0.017	0.597	0.185	0.093	0.228	0.191
86.000	-16.272	0.678	0.096	-0.496	1.613	-0.055	0.018	0.599	0.185	0.083	0.231	0.199
87.000	-16.247	0.670	0.092	-0.514	1.610	-0.076	0.018	0.601	0.185	0.074	0.233	0.208
88.000	-16.221	0.661	0.088	-0.532	1.607	-0.097	0.018	0.603	0.185	0.064	0.235	0.216
89.000	-16.195	0.651	0.084	-0.550	1.606	-0.111	0.018	0.605	0.185	0.054	0.236	0.222
90.000	-16.170	0.643	0.080	-0.568	1.606	-0.111	0.018	0.607	0.184	0.045	0.237	0.228
91.000	-16.144	0.634	0.075	-0.586	1.607	-0.107	0.018	0.609	0.184	0.035	0.237	0.232
92.000	-16.119	0.625	0.071	-0.604	1.607	-0.107	0.018	0.609	0.184	0.027	0.237	0.235
93.000	-16.093	0.616	0.067	-0.622	1.607	-0.107	0.018	0.609	0.184	0.018	0.236	0.236
94.000	-16.067	0.607	0.063	-0.640	1.607	-0.107	0.018	0.609	0.184	0.011	0.235	0.234
95.000	-16.042	0.599	0.059	-0.658	1.607	-0.107	0.018	0.609	0.184	0.005	0.233	0.230
96.000	-16.016	0.589	0.055	-0.676	1.608	-0.107	0.018	0.609	0.185	0.000	0.232	0.224
97.000	-15.991	0.581	0.051	-0.694	1.608	-0.107	0.018	0.609	0.185	0.000	0.230	0.215
98.000	-15.965	0.572	0.047	-0.712	1.608	-0.107	0.018	0.609	0.186	0.000	0.228	0.204
99.000	-15.939	0.562	0.043	-0.730	1.608	-0.107	0.018	0.609	0.186	0.000	0.227	0.191
100.000	-15.914	0.554	0.039	-0.748	1.608	-0.107	0.018	0.609	0.187	0.000	0.226	0.176
101.000	-15.888	0.545	0.035	-0.767	1.608	-0.108	0.018	0.609	0.188	0.000	0.225	0.160
102.000	-15.863	0.536	0.031	-0.785	1.608	-0.108	0.018	0.609	0.189	0.000	0.224	0.143
103.000	-15.837	0.527	0.027	-0.803	1.608	-0.108	0.018	0.609	0.190	0.000	0.224	0.127
104.000	-15.811	0.518	0.023	-0.821	1.608	-0.108	0.018	0.609	0.191	0.000	0.225	0.112
105.000	-15.786	0.509	0.019	-0.839	1.608	-0.108	0.018	0.609	0.192	0.000	0.225	0.100
106.000	-15.760	0.500	0.015	-0.857	1.608	-0.108	0.018	0.609	0.193	0.001	0.227	0.094
107.000	-15.735	0.492	0.010	-0.875	1.608	-0.108	0.018	0.609	0.194	0.003	0.229	0.094
108.000	-15.709	0.483	0.006	-0.893	1.608	-0.108	0.018	0.609	0.195	0.005	0.230	0.105
109.000	-15.683	0.473	0.002	-0.911	1.608	-0.108	0.018	0.609	0.195	0.005	0.232	0.129
110.000	-15.658	0.465	-0.002	-0.929	1.608	-0.108	0.018	0.609	0.196	0.002	0.234	0.170
111.000	-15.633	0.457	-0.006	-0.947	1.608	-0.108	0.018	0.609	0.196	0.000	0.235	0.210
112.000	-15.608	0.449	-0.010	-0.965	1.608	-0.108	0.018	0.609	0.195	0.000	0.236	0.251
113.000	-15.583	0.441	-0.014	-0.983	1.608	-0.108	0.018	0.609	0.194	0.000	0.238	0.291

blue. For example, at maximum, a decrease of 0.10 mag in visual absolute luminosity corresponds to an increase in color (toward the red) of 0.05, 0.03, and 0.04 mag in $B-V$, $V-R$, and $V-I$, respectively. Presuming that all SN Ia's have a uniform color at maximum (as has often been done) is a poor assumption that can lead to incorrect predictions, as we show elsewhere (Riess et al 1996b). In particular, the relation between intrinsic color and luminosity helps explain how absorption "corrections" have led to *increased* dispersion in Hubble diagrams and to unphysical properties derived for dust in distant galaxies (Branch & Tammann 1992; Capaccioli et al. 1990; Joëever 1982; Tammann 1987). For comparison, the color variations at maximum due to reddening for 0.10 mag of visual extinction are expected to be 0.03, 0.03, and 0.05 in $B-V$,

$V-R$, and $V-I$. Although the sense of the color changes from absorption is the same as from intrinsic variation, the values are not.

Van den Bergh (1995) noted that the relation between intrinsic $B-V$ color and luminosity predicted by the mean behavior of Höflich & Khokhlov's (1996) theoretical models agrees coincidentally with the standard reddening law. He takes advantage of this agreement to define a reddening-free luminosity that employs a single measurement of $B-V$ color to account for both the luminosity variation intrinsic to the supernova and that which results from absorption by dust. Our empirical relation between luminosity and color shows that dust and intrinsic luminosity variation do not cause exactly the same change in color. This difference may cause the increase in dispersion around the Hubble line observed after van den Bergh's prescription is applied (Riess et al. 1996b).

More than 35 days past maximum light, all supernovae exhibit nearly uniform colors. Entries in the correction templates for day 35 give differences of 0.00, 0.01, and 0.01 mag in $B-V$, $V-R$, and $V-I$ color for a 0.10 mag change in visual absolute luminosity. Detailed theoretical modeling of SN Ia's shows a similar relation between supernova color and luminosity (Höflich & Khokhlov 1996).

An alternate view of the photometric differences between intrinsically bright and dim SN Ia's is presented in Figure 2. The family of absolute B, V, R, and I light curves shows recognizable morphological variations. The B light curve family is similar in behavior to the V family; dim SN Ia's rise and fall more rapidly in B and V than bright SN Ia's. In R, the brighter SN Ia's have a "shoulder" $\sim$25 days after B maximum. For dimmer SN Ia's, this shoulder is less pronounced and disappears completely for the most underluminous objects. In the I band, the brighter SN Ia's have two maxima. The first occurs quite early, $\sim$5 days before the B-band maximum. The second, broad maximum is at $\sim$30 days after B maximum. As the luminosity of the SN Ia's decreases, a number of changes in the I-band light curve are apparent: the first maximum is later and broader, while the second maximum is dimmer and occurs earlier. For the most underluminous SN Ia's the two maxima merge into one maximum that is broad and occurs $\sim$5 days after B maximum.

The uncertainty in the empirical relations depicted in Figure 1 is discussed in § 4. These uncertainties, shown in Figure 3, quantify how useful any SN Ia data are in predicting the distance related parameters. Figure 3 also shows how well SN Ia data are expected to fit the empirical model. This point is worth emphasizing with an example. Our family of $V-R$ color curves predicts that SN Ia's with differing intrinsic luminosity will have the same color after day 60, but Figure 3 shows that this prediction is highly uncertain. Using both our empirical model and our measure of its limitations, we will optimize our measurements of SN Ia distances.

The light and color curve reconstructions in Figure 1 provide a powerful means to measure the extinction-corrected distance at every phase of supernova observation. SN Ia's appear dim because they are distant, obscured by dust, or intrinsically dim. We can distinguish between these possibilities by using the light and color curve shapes (which determine the intrinsic luminosity and color) and measuring the observed offsets (which determine the extinction-corrected distance).

3. EXTINCTION-CORRECTED DISTANCES FROM MULTICOLOR LIGHT-CURVE SHAPES

Figure 1 provides a ready guide for measuring extinction-corrected distances. Given $BVRI$ light-curve photometry, we seek the best set of curves for a fixed value of Δ that minimizes the χ^2 between model and data. The offsets between the model and the data provide the best estimates of μ_V and A_V. Rather than searching the χ^2 parameter space for a solution, we take advantage of the linearity of our model for an immediate solution.

Referring to the matrix form of the model in equation (9), we use the following definitions; $\boldsymbol{y}$ is the column of apparent magnitude measurements, $\boldsymbol{s}$ is the column of standard templates, $\boldsymbol{L}$ is the three-column matrix with correction templates and offsets, and $\boldsymbol{q}$ is the three-element column of parameters. With these definitions, we rewrite χ^2 in equation (10) as

$$\chi^2 = (\boldsymbol{y} - \boldsymbol{s} - \boldsymbol{L}\boldsymbol{q})^T \boldsymbol{C}^{-1} (\boldsymbol{y} - \boldsymbol{s} - \boldsymbol{L}\boldsymbol{q}) \, . \tag{13}$$

The analytical minimization of χ^2 with respect to the column of free parameters $\boldsymbol{q}$ gives

$$\boldsymbol{q}_{\rm best} = [\mu_V, A_V, \Delta]^T_{\rm best} = (\boldsymbol{L}^T \boldsymbol{C}^{-1} \boldsymbol{L})^{-1} \boldsymbol{L}^T \boldsymbol{C}^{-1} [\boldsymbol{y} - \boldsymbol{s}] \, . \tag{14}$$

Equation (14) measures *simultaneously* the distance and the extinction using all the available light-curve observations, reducing the reliance on any particular time of the supernova light curve. According to our definitions in equation (1) or (5), μ_V is the apparent distance modulus *uncorrected for extinction.* The extinction-corrected MLCS distance, μ, is given by $\mu_V - A_V$. The "standard candle" distance, i.e., without any correction for light-curve shape (luminosity) or reddening, is given by $\mu_V + \Delta$. This is the distance derived by correctly fitting the shape of the visual light curve to find the peak, ignoring the color excesses, and assigning the SN Ia a standard luminosity. The standard errors for the parameters in $\boldsymbol{q}_{\rm best}$ are given by the covariance matrix, $(\boldsymbol{L}^T \boldsymbol{C}^{-1} \boldsymbol{L})^{-1}$. These errors are the *fitting* errors that reflect the uncertainty in locating a light curve's best placement in Figure 1, due to the presence of noise in either the training set light curves or in the independent light curve we are trying to fit.

This approach, until now, treats the correction templates derived from our training set as if they were perfect. This is certainly not the case, since the independent distance and A_V estimates for the objects that make up the training set objects are themselves not perfect. The same type of uncertainty is seen more easily in the Phillips (1993) relation, where the light-curve decline in the first 15 days after maximum is correlated against the luminosity derived from independent distance and A_V estimates. The uncertainty in the slope of this relation must be considered when it is used. Fortunately, our correction templates are well constrained by the accuracy of the distance and A_V estimates combined with the size of the training set. The external source of error on the parameters can be found by varying the training set distances and A_V estimates in a Monte Carlo simulation to determine the effects on the fitted parameters. As expected, the external distance error increases linearly

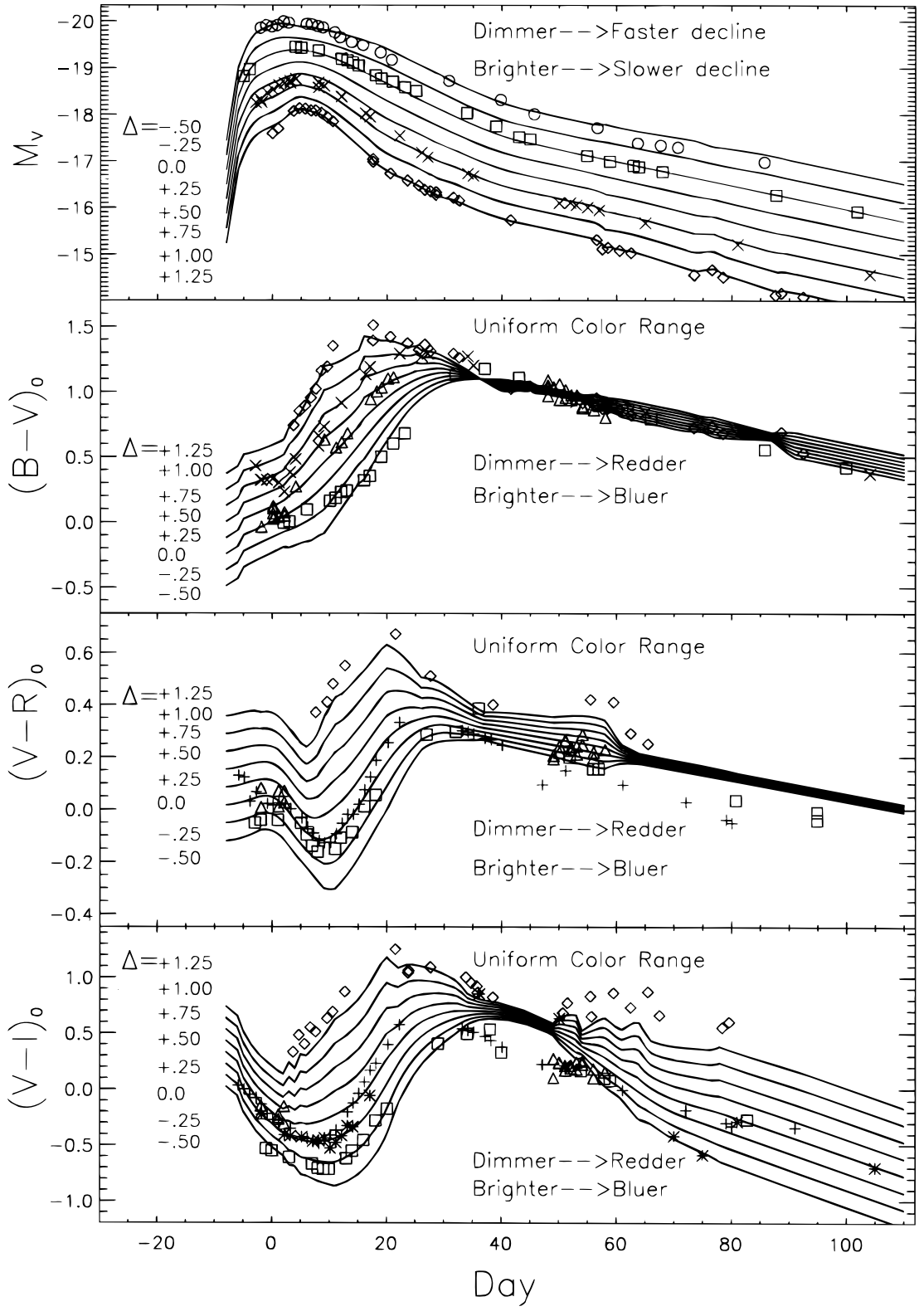

FIG. 1.—Empirical family of SN Ia light and color curves parameterized by luminosity. This sample of empirical V, $B-V$, $V-R$, and $V-I$ curves is derived from the training set and depicts the entire range of light and color curve shapes and their correlation with luminosity (on the Cepheid distance scale). This set is obtained by adding the correction templates, $R_V(t)$ or $R_{\rm color}(t)$, multiplied by various luminosity corrections, Δ, to the standard templates to make the best reconstruction of an SN Ia light and color curves. Intrinsically dim SN Ia's rise and fall faster in V and have redder colors before day 35 than intrinsically bright SN Ia's. After day 35, all SN Ia's have more uniform colors. From the multicolor light-curve shape (MLCS) method, we estimate the luminosity and extinction by dust independently from the distance to measure the extinction-free distance. Data shown as reconstructed. *Open circles:* 91T; *open squares:* 94ae; *crosses:* 86G; *open diamonds:* 91bg; *plus signs:* 92A; *triangles:* 80N.

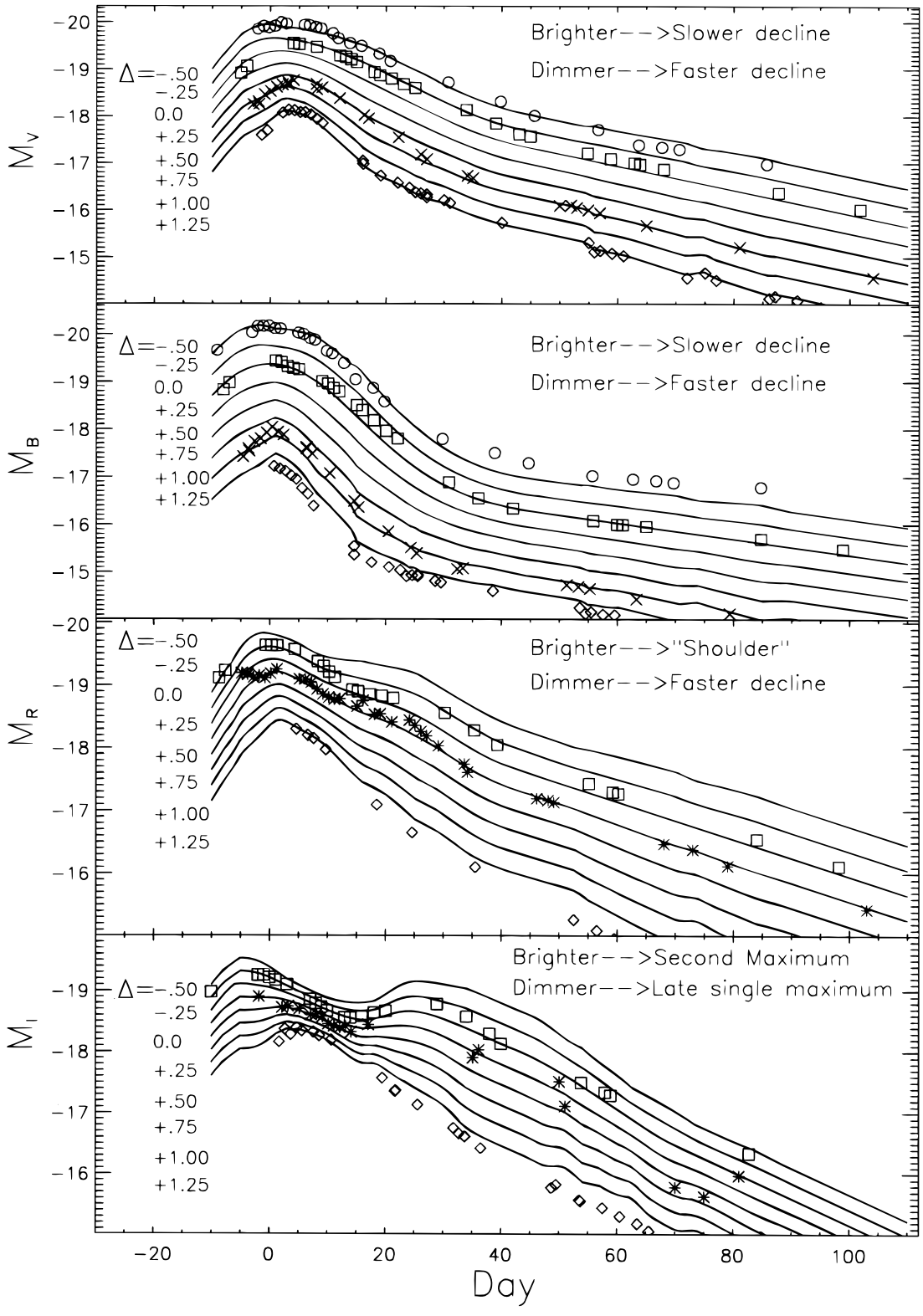

FIG. 2.—Empirical family of SN Ia *BVRI* light curves parameterized by luminosity. This family of light curves is derived in the same way as the families in Fig. 1 and shows the differences in photometric behavior for bright and dim SN Ia's. Intrinsically dim SN Ia's rise and fall faster in *B* and *V* than intrinsically bright SN Ia's. For the *R* light curve, a "shoulder" occurs ~25 days after *B* maximum in the bright SN Ia's. This shoulder is weaker for dimmer SN Ia's and is absent for the most underluminous ones. In the *I* band, the bright SN Ia's have two maxima; one early (~5 days before *B* maximum) and one later (~30 days after *B* maximum). As the luminosity of the SN Ia's decreases, the first maximum occurs later and is broader, while the second maximum is dimmer and occurs earlier. For the most underluminous SN Ia's the two maxima merge into one maximum that is broad and occurs ~5 days after *B* maximum. Data shown as reconstructed. *Open circles:* 91T; *open squares:* 94ae; *crosses:* 86G; *open diamonds:* 91bg; *plus signs:* 92A; *triangles:* 80N.

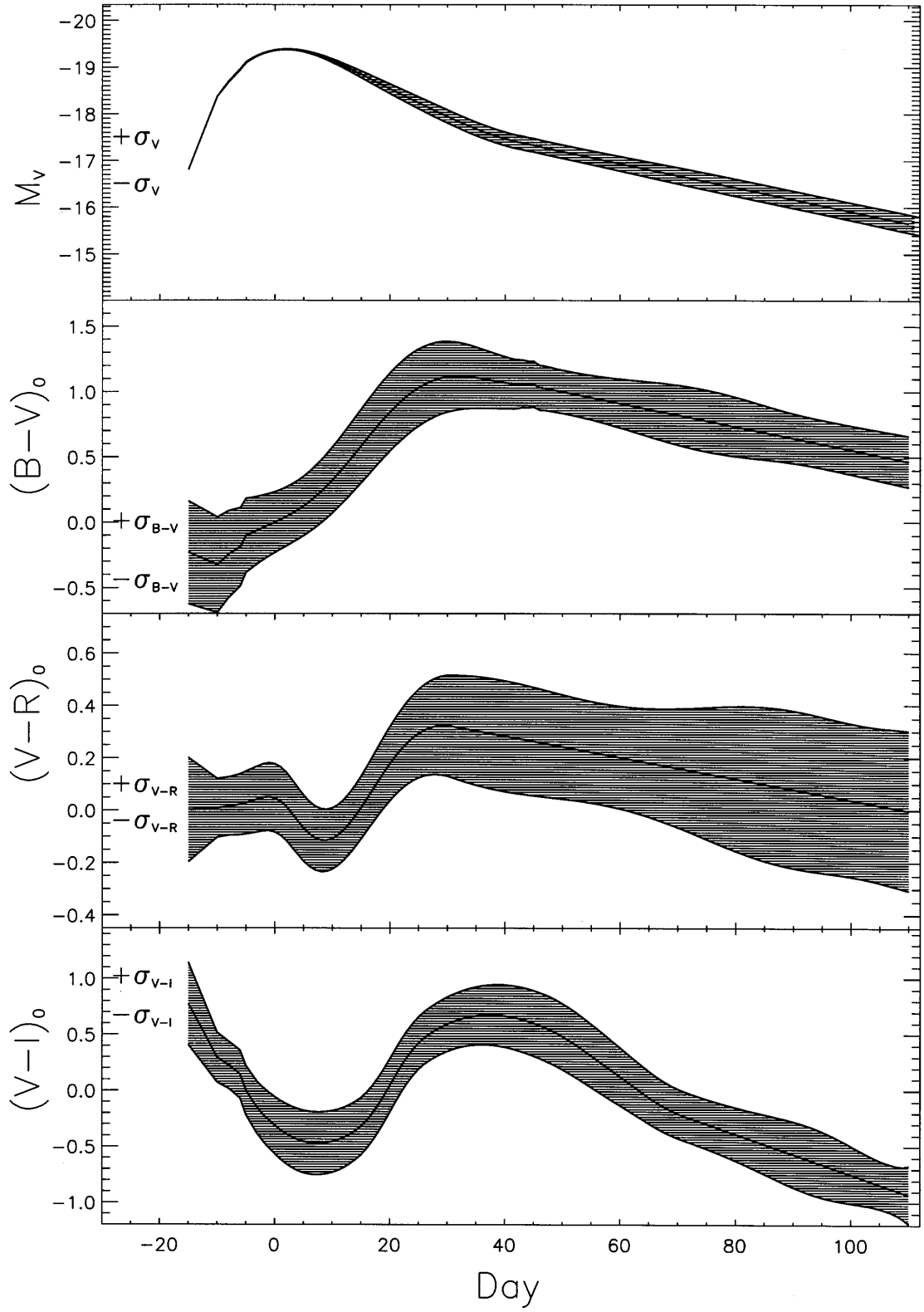

FIG. 3.—Dispersion of noise-free light and color curves around the best-fit model. The "gray snakes" comprise 1 σ confidence regions which, when plotted over a best-fit model fit (here chosen as the $\Delta = 0$ standard templates), are expected to contain 68% of noise-free data points. The square of these functions would be the diagonal entries of the signal correlation matrix ($\boldsymbol{S}$) which, added to the noise correlation matrix ($\boldsymbol{N}$), would give the model correlation matrix ($\boldsymbol{C}$). To compensate for our inability to determine either data covariance (off diagonal elements) or higher order correlations in luminosity, we rescale each of these functions as described in § 4.

with the light curve's luminosity correction, Δ, and it is well described by $\sigma = 0.055\Delta$ mag. So for a supernova whose luminosity correction $\Delta = 0.30$ mag, our external distance error would amount to less than 0.02 mag. This error is negligible for the majority of observed supernovae whose typical $|\Delta| \leq 0.50$ mag results in $\sigma \leq 0.03$ mag. This external source of error will decrease as the square root of the training set size, which we will be able to expand in the future.

The time of maximum for each supernova is a nonlinear parameter that cannot be solved for analytically in this scheme. It requires an outer iteration to minimize χ^2 in equation (13). For our well-observed light curves, the uncertainty in the time of maximum, typically well under 1 day, has a negligible effect on the parameter errors, with the median *error* increasing by only 10% if the time of maximum is varied ± 1 day. For poorly observed light curves whose observations begin ~ 10 days after maximum, the uncertainty in the time of maximum increases substantially, as does its effect on the parameter errors. We discard all light curves beginning more than 10 days after maximum to avoid SN Ia's with large uncertainties while maintaining a useful number of objects. When the set of usable SN Ia's has grown sufficiently, the precision of this distance indicator might be improved by imposing an even stricter requirement for the time of the first observation.

4. CONSTRUCTING THE CORRELATION MATRIX

The correlation matrix, $\boldsymbol{C}$, used in equations (13) and (14) to determine the best parameters and χ^2 of the light-curve fit, is the sum of two parts, $\boldsymbol{C} = \boldsymbol{S} + \boldsymbol{N}$. The noise correlation matrix, $\boldsymbol{N}$, is the correlation matrix for the measurement errors. The signal correlation matrix, $\boldsymbol{S}$, is the correlation matrix which, *in the absence of measurement error*, estimates the expected deviations of the light curves from our model. It is the $\boldsymbol{S}$ matrix that allows us to use our model despite its known shortcomings. The $\boldsymbol{N}$ matrix is supplied by the conscientious observer.

The $\boldsymbol{S}$ matrix has two parts, diagonal and off-diagonal entries, which, in principle, are estimated from our training set. The diagonal entries are estimates of the expected deviation of the light curve from the model. We determine the entries along the diagonal of each photometric band's block of $\boldsymbol{S}$ by measuring the dispersion of each training set member's R_V and $R_{\rm color}$ around the ensemble average R_V and $R_{\rm color}$ given in equations (11) and (12) minus each light curve's contribution from measurement error. The result gives, as a function of time, the expected errors of noise-corrected data around the best-fit model. We have plotted this dispersion around the best-fit model reconstruction in Figure 3 using the standard templates ($\Delta = 0$) as an example. The resulting "gray snakes" comprise 1 σ confidence regions which, when plotted over a best model fit, would be expected to contain 68% of the data points. The square root of the diagonal entries of the $\boldsymbol{S}_{\boldsymbol{V,B,R,I}}$ matrix are provided in Table 2.

The off-diagonal entries of the $\boldsymbol{S}$ matrix provide estimates of the correlation between model residuals. These correlations are likely to be considerable. There are many more elements to consider in determining the point-to-point correlations than we had for the previous autocorrelations. While initially we had only to estimate the expected model residuals for a given band on a given day of the light curve, the off-diagonal entries require much more information. We would need to estimate the amount of covariance between observations on different days in the same band, in different bands on the same day, and in different bands on different days (In addition, we would have to remove the contribution from measurement covariances, which observers generally do not supply!). Unfortunately, our sparse training set is currently inadequate for quantifying these covariances. A simple two-point correlation function suggests that these covariances are most important in B, R, and I but does not provide enough information to approximate them adequately. This is the same compromise we faced in choosing a simple linear model over one with higher order terms. A detailed description of how our data deviate from a linear model requires the same information as would be required to establish a more detailed model for our data. Either improvement requires a large training set. We echo our minimalist approach to our model with a minimalist approach to the $\boldsymbol{S}$ matrix. We employ a diagonal $\boldsymbol{S}$ matrix (with the diagonals determined as above) with compensation for the possibility that some photometric bands are more adequately modeled with our linear model than others. We increase the diagonal elements of the signal correlation matrix enough to compensate for our inability to estimate its off-diagonal terms. A simple rescaling of the entire signal correlation matrix would be less effective because some photometric bands of data (matrix blocks) have more model covariance (i.e., nonlinear behavior) than others.

We seek to weight each band's data in the correlation matrix by its ability to predict the parameter in common, Δ. This approach recognizes that in a linear model some bands may be better than others at estimating the parameter Δ and weights each light curve accordingly. To determine each band's weight, we allow their weights in the correlation matrix to vary and maximize the log-likelihood function for the determination of Δ,

$$\mathscr{L} \equiv -\frac{1}{2}\left(\chi^2_\Delta - \sum_{i=1}^{n} \ln \frac{1}{\sigma^2_{\Delta_i}}\right). \tag{15}$$

Maximizing $\mathscr{L}$ is the desired way to determine parameters of the correlation matrix in which the conventional approach of minimizing χ^2 would necessarily drive the weights and χ^2 to zero (Rybicki & Kleyna 1994). A simple exercise shows that maximizing $\mathscr{L}$ with respect to the weights drives the residuals to the smallest value they can have while still maintaining a χ^2 per degree of freedom near unity. By maximizing $\mathscr{L}$, we optimize our data's ability to predict the parameter, Δ, while requiring simultaneously that the estimated error in Δ is reasonable. Given more training set data, we could estimate the entire correlation matrix by maximizing $\mathscr{L}$. With our current limited training set, we will use our previous prescription to parameterize the diagonal blocks of the correlation matrix that correspond to each photometric filter and use $\mathscr{L}$ to determine the relative weights of those blocks.

Here $\mathscr{L}$ takes the form

$$\mathscr{L} = -\frac{1}{2}\left[\sum_{i=1}^{n} \frac{(\Delta_{\rm MLCS} - \Delta_{\rm ind})^2}{\sigma^2_{\Delta_{\rm MLCS}} + \sigma^2_{\Delta_{\rm ind}}} - \sum_{i=1}^{n} \ln\left(\frac{1}{\sigma^2_{\Delta_{\rm MLCS}} + \sigma^2_{\Delta_{\rm ind}}}\right)\right], \tag{16}$$

where the subscripts "ind" and "MLCS" denote the value and uncertainty of Δ as determined by independent methods and MLCS, respectively. Optimal weighting of the B, V, R, and I data minimizes the difference between the independently determined Δ values (in Table 1) and the MLCS predicted Δ values that are a function of the weights in the $\boldsymbol{C}$ matrix. Using equation (16) and a downhill simplex method (Press et al. 1992) to find its maximum, we have determined the relative weights

of each band. The diagonal $\boldsymbol{C}_{\boldsymbol{V},\boldsymbol{B},\boldsymbol{R},\boldsymbol{I}}$ matrix needed for the MLCS fit comes from adding the square of the model errors in Table 2 to the square of the observers' photometry errors, then multiplying the four diagonal blocks of $\boldsymbol{C}_{\boldsymbol{V},\boldsymbol{B},\boldsymbol{R},\boldsymbol{I}}$ by 0.37, 11.45, 8.85, and 5.52. These values, determined by maximizing equation (16), indicate that the V-band light curves are significantly better predictors of Δ than B, R, or I data within the framework of our linear model. Specifically, a V-band observation contributes 5.6, 4.9, or 3.9 times as much as a B-, R-, or I-band observation toward determining the luminosity correction for an SN Ia. This result is not astonishing, since it is well established that light curves in B, R, and I with differing luminosity can cross each other (Suntzeff 1993). A crossing point of such light curves implies the same light or color curve shape for SN Ia's with different Δ values. Such behavior found in B, R, and I diminishes their predictive power in our linear model, but the independence of their A_V measurements provides useful estimates of extinction.

We have assumed that the correlation matrix for V, B, R, and I data is diagonal, but the correlation matrix for V, $B-V$, $V-R$, and $V-I$ is certainly not diagonal, since an observation of m_V and m_{B-V} made at the same time are anticorrelated with covariance $-\sigma_V^2$. Formation of the correlation matrix for V, $B-V$, $V-R$, and $V-I$ data, i.e., $\boldsymbol{C}_{\boldsymbol{V},\boldsymbol{B}-\boldsymbol{V},\boldsymbol{V}-\boldsymbol{R},\boldsymbol{V}-\boldsymbol{I}}$, may be done directly with care to include the covarience terms of $\pm\sigma_V^2$ or by means of a simple rotation. This involves writing down the rotation matrix, $\boldsymbol{A}$, which satisfies

$$\boldsymbol{A}\begin{pmatrix} V \\ B-V \\ V-R \\ V-I \end{pmatrix} = \begin{pmatrix} V \\ B \\ R \\ I \end{pmatrix}, \tag{17}$$

and we readily identify

$$\boldsymbol{C}^{-1}_{\boldsymbol{V},\boldsymbol{B}-\boldsymbol{V},\boldsymbol{V}-\boldsymbol{R},\boldsymbol{R}-\boldsymbol{I}} = \boldsymbol{A}^T\boldsymbol{C}^{-1}_{\boldsymbol{V},\boldsymbol{B},\boldsymbol{R},\boldsymbol{I}}\boldsymbol{A}\ . \tag{18}$$

Deriving the desired correlation matrix from equation (18) has the advantage of requiring the much simpler $\boldsymbol{A}$ and diagonal $\boldsymbol{C}^{-1}_{\boldsymbol{V},\boldsymbol{B},\boldsymbol{R},\boldsymbol{I}}$ matrices.

Meaningful model parameter errors can only come from models that fit the data within statistical expectations. We require that both the V light-curve model and the color curve models give a reduced (per degree of freedom) χ^2 of 1. To define the confidence region for the distance parameters, we use the covariance matrix of the fit, $(\boldsymbol{L}^T\boldsymbol{C}^{-1}\boldsymbol{L})^{-1}$, multiplied by the *reduced* χ^2 of the light or color curve fits that measures the parameter of interest. This, in effect, is renormalization of the $\boldsymbol{C}$ matrix, now done on a supernova-by-supernova basis. This renormalization is not generally a large factor and would presumably become unnecesary with a better nondiagonal model for $\boldsymbol{C}$.

In the case of the distance modulus error, derived from the visual band data, the error is the (1, 1) entry of the covariance matrix multiplied by the reduced χ^2 of the V light curve fit:

$$\sigma^2_{\mu_V} = (\boldsymbol{L}^T\boldsymbol{C}^{-1}\boldsymbol{L})^{-1}_{1,1}\,\chi^2_\nu(V)\ . \tag{19}$$

Similarly, the extinction error, as derived from the $B-V$, $V-R$, $V-I$, is the (2, 2) entry of the covariance matrix multiplied by the reduced χ^2 of the color curves' fit:

$$\sigma^2_{A_V} = (\boldsymbol{L}^T\boldsymbol{C}^{-1}\boldsymbol{L})^{-1}_{2,2}\,\chi^2_\nu(B-V,\ V-R,\ V-I)\ . \tag{20}$$

The extinction-corrected distance is given by $\mu_V - A_V$, and its variance is the sum of equations (19) and (20) minus twice the covariance of the estimates of μ and A_V:

$$\sigma^2_{\mu_V - A_V} = \sigma^2_{\mu_V} + \sigma^2_{A_V} - 2(\boldsymbol{L}^T\boldsymbol{C}^{-1}\boldsymbol{L})^{-1}_{1,2}\sqrt{\chi^2_\nu(V)\chi^2_\nu(B-V,\ V-R,\ V-I)}\ . \tag{21}$$

The extinction-corrected distance error of equation (21) is the previously mentioned fitting error. For a particular SN Ia, its size depends on light-curve sampling, measurement errors, and light-curve shape (see § 6). These errors provide useful individual estimates of distance uncerainty.

5. FORMALIZED TRUNCATION OF A_V

What is the best way to estimate the absorption by dust given a measurement of excess color? We have well-founded a priori knowledge that dust scatters or absorbs light but does not amplify it, so the true value of A_V must lie within the range

$$0 \le A_V \le (\mu_V + M_V - m_{\rm lim})\ , \tag{22}$$

where $m_{\rm lim}$ is a detection limit. Since we measure A_V by dust's reddening effect, we say, a priori, that dust cannot "blue-en" or brighten an SN Ia. We could use this knowledge to improve our estimate of A_V by truncating any measurement of A_V found to be less than zero. Simple truncation carries the disadvantage of improperly treating our useful estimate of σ_{A_V} from equation (20). What is the best way to use our estimate of A_V and its error together with prior knowledge that A_V cannot be less than zero? A straightforward Bayesian calculation provides the solution.

Suppose we were to make an estimate of A_V with value $\hat{a}$ and normal error $\sigma_{\hat{a}}$. Further, we have some knowledge of the distribution of the *observed* A_V, $p(A_V)$. Using Bayes's theorem,

$$p(A_V \mid \hat{a},\ \sigma_{\hat{a}}) = \frac{p(\hat{a} \mid A_V,\ \sigma_{\hat{a}})p(A_V)}{p(\hat{a})} = \frac{\exp\,[-(A_V - \hat{a})^2/2\sigma^2_{\hat{a}}]p(A_V)}{\int_0^\infty p(A_V)\exp\,[-(A_V - \hat{a})^2/2\sigma^2_{\hat{a}}]dA_V}\ . \tag{23}$$

This "Bayesian filter" provides a probability distribution for the *true* A_V from which we can obtain a best estimate of A_V and its error. A minimalist approach to $p(A_V)$ would be to assume it is constant over the range in equation (22). This

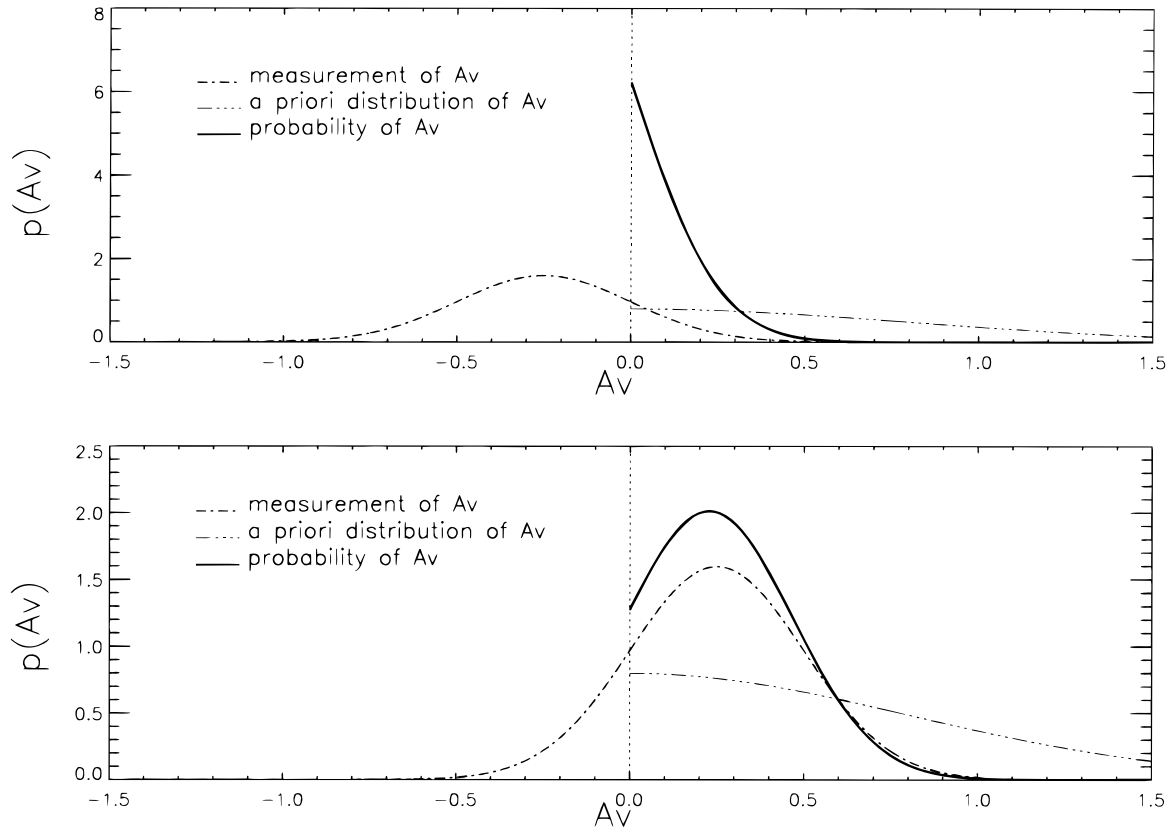

FIG. 4.—Bayesian estimation of visual extinction by dust. By combining our MLCS measurement of visual extinction, A_V, and its error with a priori knowledge that A_V is positive, we can estimate the likelihood and distribution of the *true* value for A_V. *Top:* Combination of a *negative* estimate for A_V ($= -0.25 \pm 0.20$) with a Gaussian wing ($\sigma = 1$) a priori distribution to yield an estimate for A_V ($= 0.0 \pm 0.08$). *Bottom:* Combination of a *positive* estimate for A_V ($= 0.25 \pm 0.20$) with the same a priori distribution to give an estimate for A_V ($= 0.24 \pm 0.16$).

formalized truncation is too conservative and unrealistic, and we can do better. Since supernovae with very large values of A_V are less likely to be part of a sample of detected supernovae, we suggest that a reasonable form for the *observed* $p(A_V)$ is a one-sided Gaussian that has a maximum at $A_V = 0$ and declines for large A_V (see Fig. 4). We have chosen $\sigma = 1$ mag of A_V for our $p(A_V)$, but we show in § 7 that our results are insensitive to the particular value used for σ.

6. COMPARING DISTANCES

The above completes our development of an algorithm to measure extinction-corrected distances with multicolor light-curve shapes. There are, however, a few complications to consider in the practice of measuring distances to supernovae with light-curve shapes.

The "*K*-correction" (Oke & Sandage 1968; Humason, Mayall, & Sandage 1956) corrects for the effects of redshift on the measured flux through a filter of fixed spectral response. These corrections can be approximated by measuring the effect of redshifting the spectra of SN Ia supernovae for different redshifts and phases. We can include *K*-corrections in our templates given the redshift or include them in our measurements given the redshift, using an assumed time of maximum in the outer iteration. For *B*- and *V*-band data, we have used the *K*-corrections of Hamuy et al. (1993b), and for *R* and *I* we have calculated our own (see Filippenko et al. 1996). The light curves are also affected by time dilation, so we contract the light curve by $(1 + z)$ to return it to the rest frame (Leibundgut et al. 1996; Goldhaber et al. 1996).

Using equation (14), we now measure the distance related parameters for a set of well-observed SN Ia's assuming that they share the same behavior as our training set. By applying the method as developed for the training set to this independent sample, we compute distances for each supernova and construct a Hubble diagram. Analysis of this diagram shows that the MLCS approach gives better precision than the standard candle method. We will also compare the results with a sample selected by the same criteria used by Tammann & Sandage (1995) to see whether MLCS improves the utility of a "normal" set of SNIa's. We restrict our attention to light curves obtained on a modern photometric system in which the light curve begins within 10 days of maximum light (as determined by our fit). Tests on the training set have shown that in order for a light curve to contain luminosity information in its shape, the first observation must be within 10 days of maximum. Every one of the SN Ia's in our samples was recorded on digital images and has accurate subtraction of the host galaxy background to ensure that the light-curve shapes are free from systematic errors (Boisseau & Wheeler 1991).

Our independent set of 20 supernovae contains 10 objects from the Calan/Tololo survey (Hamuy et al. 1993a, 1994, 1995, 1996; Maza et al. 1994), two from the literature (Ford et al. 1993), and eight from our own work (Riess et al. 1996a). Table 3 contains SN Ia MLCS parameters. Host galaxy redshifts (col. [2]) are in the CMB rest rame. The heliocentric redshifts (Riess et al. 1996a; Ford et al. 1993; Hamuy et al. 1995) are transformed to the Local Group rest frame by the addition of

TABLE 3

SN Ia PARAMETERS

SN Ia (1)	log v (km s^{-1}) (2)	$\mu_V - A_V$ (3)	$\sigma_{\mu_V - A_V}$ (4)	Δ (5)	A_V (6)	Galactic A_V (7)
1992bo	3.734	34.59	0.07	0.51	0.00	0.00
1992bc	3.779	34.75	0.05	−0.23	0.00	0.00
1992K	3.521	33.53	0.15	1.25	0.01	0.23
1992aq	4.481	38.27	0.06	0.35	0.00	0.00
1992ae	4.350	37.79	0.09	−0.05	0.00	0.04
1992P	3.896	34.50	0.08	−0.20	0.11	0.00
1992J.....	4.140	36.75	0.14	0.35	0.18	0.15
1991U	3.991	35.70	0.17	−0.41	0.75	0.20
1991ag	3.613	34.15	0.08	−0.27	0.01	0.13
1990af.....	4.178	36.87	0.06	0.27	0.00	0.05
1992G	3.299	32.22	0.11	0.02	0.45	0.04
1991m	3.389	32.96	0.10	0.73	0.00	0.01
1993ae	3.709	34.52	0.11	0.38	0.00	0.10
1994M	3.859	35.32	0.09	0.21	0.00	0.00
1994S	3.685	34.24	0.05	−0.13	0.00	0.00
1994T	4.030	36.16	0.10	0.33	0.00	0.00
1994Q	3.938	35.86	0.13	−0.28	0.25	0.05
1993ac	4.170	36.93	0.22	0.34	0.20	0.45
1995D	3.398	32.76	0.06	−0.28	0.21	0.00
19995E.....	3.547	33.76	0.06	−0.17	1.86	0.00

(−30, 297, −27) km s^{-1} in Galactic Cartesian coordinates (de Vaucouleurs et al. 1991; Lynden-Bell & Lahav 1988). These Local Group redshifts are transformed to the CMB rest frame with the addition of (10, −542, 300) km s^{-1} (Smoot et al. 1992). For Sn 1993ae, we have used the redshift of Abell 194 (Chapman 1988), of which the host galaxy is a member. For the three SN Ia's with $cz \leq 3000$ km s^{-1} (SN 1991M, SN 1992G, and SN 1995D), we have corrected their redshifts for their likely infall toward Virgo (Schmidt, Kirshner, & Eastman 1992).

The Galactic extinction measures (col. [7]) that we use for comparison to our own are from Burstein & Heiles (1982). The values of $\mu_V - A_V$ and $\sigma_{\mu_V - A_V}$ in columns (3) and (4) are the MLCS extinction-corrected distances and the fitting errors with the former placed onto the Cepheid variable distance scale as described in § 7 and Table 5. The line-of-sight extinction estimate, A_V, is listed in column (6), and adding it to the values of $\mu_V - A_V$ gives the distance estimate without any correction for absorption. Adding these values of μ_V to the luminosity correction, Δ, in column (5) gives a distance estimate without correction for either the luminosity–light curve relation or absorption.

In Figure 5 we show the multicolor light-curve shape reconstruction for three SN Ia's (Riess et al. 1996a) from our independent sample spanning the range of data quality and distance error. For SN 1993ac, we have 23 observations (six epochs) beginning shortly after maximum light, resulting in an extinction-corrected distance error of 0.20 mag. The light and color curves of SN 1994Q contain 42 observations (13 epochs) beginning shortly after maximum and give an extinction-corrected distance error of 0.13 mag. SN 1995D has one of the best sampled light and color curves with 107 observations (28 epochs) beginning before maximum light and yielding an extinction-corrected distance error of 0.06 mag. In general, the size of our predicted extinction-corrected distance error depends on the number of observations, the noise in the observations, and whether the SN Ia was discovered before or after maximum light. Half of our independent sample of 20 SN Ia's were observed at or before maximum light.

First we will use the Hubble diagram as an analytical tool, without reference to a distance scale calibration, to determine the precision of our method. Figure 6 shows, for comparison, two Hubble diagrams for this independent set of supernovae. In Figure 6*a* we have fit the best light-curve shape to each supernova to estimate the distance *without any correction for intrinsic luminosity variation or extinction.* In Figure 6*b* we have plotted the MLCS extinction-corrected distances to each SN Ia that accounts for intrinsic luminosity variation and extinction (see Table 3). The reduction in dispersion is dramatic. The improvement in distance precision comes from deriving the correlation between luminosity and light and color curve shape from our training set of SN Ia's and then applying these relations to the independent sample. Because the training set and the independent set have no overlapping members, the reduction in dispersion is a powerful demonstration of the effectiveness of the MLCS method.

Table 4 compares the distance estimates for different assumptions by measuring the dispersion and χ^2 on the Hubble diagram. In each case we have made a custom reconstruction of the light and color curves. The first row is the "standard candle" assumption, for which we disregard the light curve shape-luminosity correction, Δ, by adding it back to the distance, $\mu_V + \Delta$, and we make no correction for extinction. Next, we use the MLCS distance modulus, μ_V, which includes the luminosity information, but we make no allowance for absorption. Following this, we include a correction for only the Galactic component of extinction by using the Burstein & Heiles (1982) absorption measures. Finally, we use the full MLCS method to estimate the extinction-corrected distance. We compare the different methods for three different subsamples: all 20 SN Ia's, all SN Ia's minus the single most highly reddened object (SN 1995E), and with a color cut (Vaughan et al. 1995; Tammann & Sandage 1995; Hamuy et al. 1995) that discards objects outside the color range $-0.25 \leq (B-V)_{\max} \leq 0.25$, leaving 18 objects.

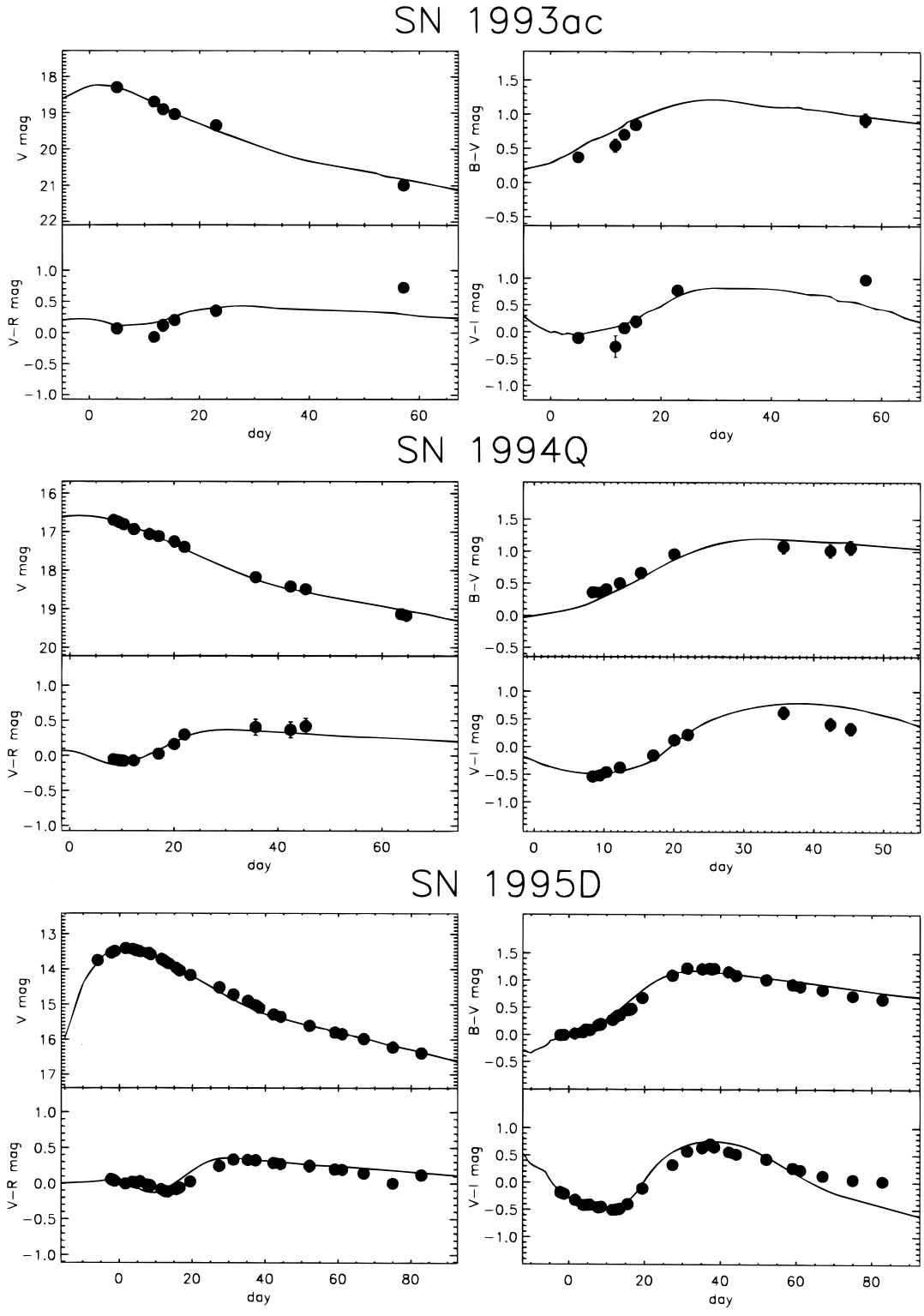

FIG. 5.—Three SN Ia MLCS fits spanning the range of data quality in the independent sample of 20 SN Ia's SN 1993ac has 23 noisy observations (six epochs) beginning shortly after maximum light, resulting in a distance error of 0.20 mag. SN 1994Q has 42 observations (13 epochs) with low noise beginning after maximum and has a distance error of 0.13 mag. SN 1995D has 107 observations (28 epochs) with little noise beginning before maximum, resulting in a distance error of 0.06 mag. Photometry is from Riess et al. (1996a).

Moving down Table 4, each successive row represents a refinement in our distance measuring technique. The result of successive improvements in the method can be seen in the decreasing dispersion on the Hubble diagram. Including the heavily reddened SN 1995E in the sample demonstrates the power of MLCS in dealing correctly with reddened objects but masks the gradual improvement in distance to be made from various aspects of the method. It is important to note that even the distances of the color cut sample can be improved with MLCS. This shows that the distance precision of "normal" or

TABLE 4

SN Ia Distance Comparisons (CMB Frame, $\sigma_{vel} = 3000$ km s^{-1})

Correction			All SN Ia's, $N = 20$		Without SN 1995E, $N = 19$		Color Cut, $N = 18$	
Luminosity	A_V	Form	σ	P_r	σ	P_r	σ	P_r
None	None	$\mu_V + \Delta$	0.52	...	0.40	...	0.33	...
MLCS.....	None	μ_V	0.46	0.015	0.20	$<1 \times 10^{-6}$	0.20	2×10^{-5}
	Galactic	$\mu_V - A_{V,gal}$	0.46	0.25	0.17	0.018	0.16	0.0085
	MLCS	$\mu_V - A_V$	0.12	1×10^{-5}	0.13	7×10^{-5}	0.13	0.00013

"Branch-normal" SN Ia's can be enhanced significantly using light and color curve information. The MLCS method is not just "reining in" the extreme SN Ia's but rather it is improving the distance measures to all the SN Ia's.

To demonstrate the statistical significance of each level of improvement, we have included in Table 4 the probabilities, P_r, that the observed improvement in dispersion could occur from a *random* set of distance corrections. These probabilities give the likelihood for the null hypothesis, that our distance "corrections" have no relation to the true SN Ia distances. In a Monte Carlo simulation, we apply a set of random corrections chosen from the distribution of proposed corrections and see how often the dispersion is as low or lower than the actual improved dispersion. The value of P_r gives the probability that the observed (or a greater) decrease in dispersion for each successive distance refinement occurred by chance. The results show that MLCS luminosity and extinction corrections are highly significant regardless of the sample criterion. Both the MLCS luminosity correction and extinction correction reject strongly the null hypothesis that they are unrelated to the true distance of the SN Ia's. Even the small corrections for galactic extinction do more good than harm. Yet, accounting only for the Milky Way's contribution to the total absorption fails to account for host galaxy extinction, which in a few cases can be substantial. Using all the predictive power of MLCS gives remarkably low values for the dispersion with an exceedingly small probability that this improvement in dispersion occurred by chance. With a conservative estimate for the peculiar velocity associated with each field galaxy of 300 km s^{-1}, our observed dispersion of 0.12 mag implies a typical distance precision of 5%. The improvement in distance precision by including a correction for host galaxy extinction with the conventional reddening law is the first demonstration that such corrections can be made successfully.

Our Monte Carlo simulation demonstrates that even for a set of SN Ia's selected by color, such as those used by Sandage et al. (1996), the MLCS method makes a significant improvement in the precision of the distances. For the color cut sample, the probability that both our luminosity and extinction corrections would improve the dispersion from 0.33 to 0.13 mag by chance is *less than one in a million.*

Both SN 1992K and SN 1995E provide instructive examples of how this method leads to improved distance estimates. Both objects appear to be dim, which for a standard candle suggests that they are at a great distance. Assuming a standard candle luminosity places each of them much further away than their redshift implies (see Fig. 6*a*). Yet, there are clues in the light and color curves of these objects that indicate that they are dim for different reasons. The rapidly declining V light curve of SN 1992K and the color evolution of its $B-V$ curve are nearly identical to the photometric behavior of the subluminous SN 1991bg, a member of the training set (Hamuy et al. 1994). Application of the MLCS method estimates SN 1992K to be $\Delta = 1.25$ mag dimmer than the standard SN Ia, though its A_V is only 0.01 mag. This correction to the luminosity is independent of the SN's redshift since it depends only on the light-curve shape, but it is reassuring to note that accounting for this object's intrinsic faintness shifts its distance quite precisely onto the Hubble line.

For the case of SN 1995E, the dim appearance that places this SN Ia below and to the right of the Hubble line is not intrinsic to the supernova, but rather is a result of absorption, as shown by MLCS. This supernova was found on the spiral arm of NGC 2441. The shape of its light and color curves suggest a fair resemblance to the standard SN Ia event ($\Delta = -0.17$ mag), but all its measured colors are displaced systematically to the red, as would occur from absorption by dust. By fitting the *shape* of the color curves independently from the *value* of the color, we can measure the color excesses. Assuming a standard reddening law (see Riess et al. 1996b), we estimate the visual band extinction to be 1.86 mag. As in the case of SN 1992K, correcting the luminosity of SN 1995E makes its distance consistent with its redshift measurement. Using a color cut requiring $-0.25 \leq (B-V)_{max} \leq 0.25$, both these objects would be discarded. Yet, we can keep these objects (and others like them) in the sample and use the MLCS method to distinguish between supernovae that are intrinsically dim and those that are dimmed by dust absorption.

We can make two significant checks of our extinction-corrected distances by examining the fit of the Hubble line to the data. We examine the linearity of the Hubble law by measuring the slope of the relation between the MLCS distance modulus and the logarithm of the redshift. Assuming that space is Euclidean for our modest redshifts, the expectation of this slope is 0.2. Lauer & Postman (1992) found a slope of 0.1992 ± 0.006 using brightest cluster galaxies, and Jerjen & Tammann (1993) found a slope of 0.1988 ± 0.006 using the mean of a number of distance indicators to fifteen clusters. Using the extinction-corrected distances and errors of Table 3 yields a slope of 0.2010 ± 0.0035, which is consistent with 0.2 and with the two previous results. The small error on our slope over the distance interval $32.2 < \mu < 38.3$ makes this the most precise check of this classical test of cosmology. Finally, we can examine the goodness of fit of our Hubble line to the extinction-correction MLCS distances. The χ^2 of the fit using the independently determined distance errors in Table 3 and $\sigma_{vel} = 300$ km s^{-1} is 13 for 19 degrees of freedom, which is within the expectation of χ^2. The value of χ^2 is strongly dependent on the assumed random velocity of the field galaxies hosting our SN Ia due to our low dispersion and small distance errors. A random velocity error for our field galaxies in the range 125 km s^{-1} $\leq \sigma_{vel} \leq$ 300 km s^{-1} gives a χ^2 within its likely range of 13–25 and is consistent with other determinations of this random velocity component (Marzke et al. 1995; Davis & Peebles 1983). All indications

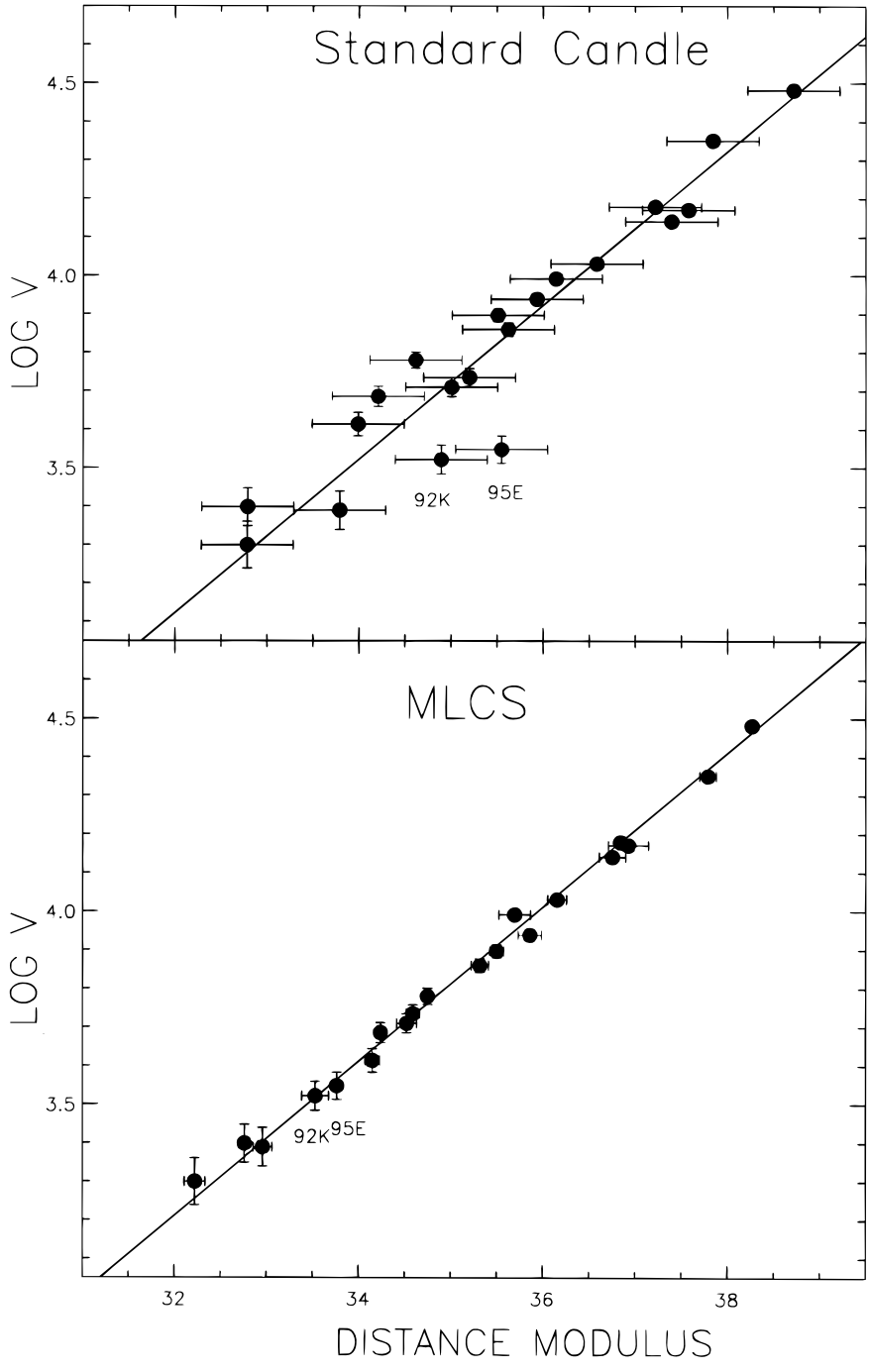

FIG. 6.—Hubble diagrams for SN Ia's with velocities in the *COBE* rest frame on the Cepheid distance scale (Sandage et al. 1994, 1996). All velocity errors are 300 km s^{-1}, reflecting a plausible estimate of random velocities with respect to the Hubble flow. (*a*) Distances estimated with a standard luminosity assumption and no correction for extinction. This method yields $\sigma_v = 0.52$ and $H_0 = 52 \pm 8$ (statistical) km s^{-1} Mpc^{-1}. (*b*) Distances from the MLCS method, which makes a correction for intrinsic luminosity variation and total extinction as determined from the light and color curve shapes. This method yields $\sigma_v = 0.12$ and $H_0 = 64 \pm 3$ (statistical) km s^{-1} Mpc^{-1}.

suggest that the MLCS method provides remarkably precise, extinction-corrected distances that are a significant improvement over SN Ia distances from previous methods.

7. DISCUSSION

Our intent has been to describe the MLCS method in enough detail so others can take advantage of the precise distance estimates it provides. The strength of MLCS lies in its ability to disentangle the effects of absorption and intrinsic luminosity variations while providing meaningful error estimates. These measures are derived from the distance-independent observables of multicolor light-curve shapes. The accuracy of the MLCS *relative* distance measures has been well established on an independent set of 20 SN Ia's on the Hubble diagram.

TABLE 5

SN Ia Distance Calibration

SN Ia (1)	$\mu_{MLCS}(\sigma)$ (2)	$\mu_{Ceph}(\sigma)$ (3)	$\mu_{MLCS} - \mu_{Ceph}(\sigma)$ (4)	$\Delta(\sigma)$ (5)	$M_V - M_{V,\,81B}(\sigma)$ (6)
1972E	27.21[a](0.09)	28.08[a](0.10)	0.87(0.13)	−0.33(0.04)	−0.28(0.21)
1981B	30.38(0.07)	31.10(0.20)	0.72(0.21)	0.01(0.04)	0.00(0.00)
1990N.....	31.04(0.14)	32.00(0.27)	0.96(0.27)	−0.27(0.04)	−0.07(0.23)

[a] Distance modulus uncorrected for extinction.

To place our MLCS distances on the established *absolute* distance scale, we use the luminosity calibration for a number of SN Ia's with an independent distance indicator of high precision. At present, there are three SN Ia's whose light curves meet our MLCS quality criteria (modern photoelectric photometry with observations less than 10 days after maximum) and whose distances have been measured with Cepheids observed with the *Hubble Space Telescope.*

The three SN Ia's, SN 1972E, SN 1981B, and SN 1990N, are listed Table 5: column (2) gives the extinction-corrected MLCS distances on the distance scale of SBF-PNLF-TF (Table 1), column (3) gives best distances as determined by *HST* Cepheid measurements (Sandage et al. 1994, 1996), column (4) gives the differences between columns (3) and (2), column (5) gives the MLCS luminosity correction, and column (6) gives the Sandage et al. (1996) M_V minus the M_V for the "standard" shape SN 1981B. By comparing our precise MLCS *relative* distances to the trustworthy Cepheid *absolute* distances, we see a consistent difference of 0.84 ± 0.10 mag. Adding this difference to all our distance estimates places our distance indicator on the Cepheid distance scale. Further, it provides an absolute luminosity calibration for the standard ($\Delta = 0$) SN Ia of $M_V = -19.36 \pm 0.10$ mag at B maximum. This calibration for the standard M_V template is used in Table 2. The extinction-corrected distances listed in Table 3 include this offset, which places them on the Cepheid distance scale. We can calculate the Hubble constant by fitting

$$\log v = 0.2(\mu_V - A_V) + \log H_0 - 5 \tag{24}$$

to the distances and velocities in Table 3 using the tabulated errors $\sigma_{\mu_V - A_V}$ and an assumed random velocity of 300 km s^{-1}. The result is a Hubble constant of 64 ± 3 km s^{-1} Mpc^{-1} where the uncertainty is internal and incorporates a 0.03 mag uncertainty in the Hubble line and a 0.10 mag uncertainty in the placement onto the Cepheid distance scale. We see also that the MLCS luminosity corrections (col. [5]) are consistent with the luminosity differences as determined by the Cepheids (col. [6]).

For comparison, we perform the same calculation for the distance and extinction methods using the three SN Ia samples. We apply each method to the calibration set to determine the offset onto the Cepheid scale and to the distant set to determine the Hubble line. For the methods that do not provide their own error estimates, we assume a constant distance error of the size necessary to obtain the expected χ^2 of the fit to the Hubble line. In Table 6 we list the determinations of the Hubble constant and internal error for the different methods and samples.

The color cut sample provides us with a set of SN Ia's that are directly comparable to the "normal" set used by Sandage et al. (1996). Using the assumption of a standard luminosity, the color cut sample gives $H_0 = 55 \pm 5$ km s^{-1} Mpc^{-1}, which is consistent with the Sandage et al. (1996) values of $H_0(B) = 56 \pm 4$ and $H_0(V) = 58 \pm 4$ km s^{-1} Mpc^{-1} obtained with the same standard brightness assumption and sample criteria, though with a different set of light curves.

In § 6 and Table 4, we demonstrate that each of the distance measuring improvements en route to the complete MLCS method is highly significant and should be employed to obtain the best result. Using the MLCS method to measure extinction-corrected distances and errors yields a Hubble constant of $H_0 = 64 \pm 3$ km s^{-1} Mpc^{-1} or $H_0 = 63 \pm 3$ km s^{-1} Mpc^{-1} using constant weighting. The only significant change in the Hubble constant arises from including the luminosity correction, Δ. This is because the mean luminosity of the three nearby calibrators is $\sim$15% brighter than the mean luminosity of the 20 SN Ia's in the distant sample. That these nearby SN Ia's are brighter than the distant SN Ia's *does not necessarily* imply an antiselection bias because our sample is neither volume nor magnitude limited. If our sample was complete in volume or magnitude, we would observe a tremendous increase in the number of observed SN Ia's at large distances. Figure 6 shows that this is clearly not the case. We elaborate on this point below.

A complete error budget for any of the values of H_0 in Table 6 would consist of the stated internal error added in quadrature to the estimated uncertainty in the Cepheid zero point, roughly 0.15 mag (Feast & Walker 1987). For the MLCS extinction-corrected distances, this gives a value of $H_0 = 64 \pm 6$ km s^{-1} Mpc^{-1}.

TABLE 6

SN Ia Hubble Constant Comparisons (CMB Frame, $\sigma_{vel} = 300$ km s^{-1})

Correction			H_0		
Luminosity	A_V	Form	All SN Ia's, $N = 20$	Without SN 1995E, $N = 19$	Color Cut, $N = 18$
None	None	$\mu_V + \Delta$	52 ± 8	54 ± 6	55 ± 5
MLCS.....	None	μ_V	61 ± 9	63 ± 4	62 ± 4
	Galactic	$\mu_V - A_{V,\,gal}$	63 ± 9	64 ± 4	63 ± 4
	MLCS	$\mu_V - A_V$	64 ± 3	64 ± 3	64 ± 3

The MLCS distances to SN Ia's in the Hubble flow combined with redshifts provide the necessary information to estimate the peculiar velocity component of each object's radial motion. Plotted on the sky, the velocity residuals show a dipole pattern indicative of the motion of the Local Group with respect to a frame defined by the supernovae. Our preliminary analysis of this motion with a subset of 13 supernovae from the current set and without our MLCS reddening information was consistent with convergence to the cosmic microwave background frame and inconsistent with the Lauer & Postman (1994) frame at 7000 km s^{-1} (Riess et al. 1995b). The same analysis performed at higher precision using the independent set of 20 SN Ia's and the MLCS method (which now includes extinction corrections) yields an even stronger detection of the Local Group motion with similar results. In the future, when the sample of SN Ia's has grown, we will revisit our analysis of the Local Group motion from SN Ia's.

Sections 2–5 outline the MLCS technique in sufficient detail to allow for future redetermination of the necessary templates and functions as more supernovae become available or are deemed desirable to include in the training set. The training set for this paper uses all supernovae for which accurate and extensive photoelectric photometry is currently available, as well as definitive relative distance estimates and A_V estimates. These include, from the Phillips (1993) set, SN 1980N, SN 1981B, 1986G, 1989B, 1990N, 1991T, 1991bg, and 1992A. We exclude SN 1971I, for which only photographic photometry is available. We also use SN 1994ae (Riess et al. 1996a), for which there are detailed photometric light curves and an independent distance (Dell'Antonio 1995). Ideally we would use only SN Ia's with no evidence of extinction, but currently we lack a sufficient number of training set objects to discard any. Instead, we estimate A_V from the color differences of unreddened SN Ia's of similar light-curve shape and propagate the resulting uncertainty in A_V to our distance errors.

It is also likely that in time, the distance estimates used for the training set may improve. Most recently, some of the distance estimates provided by surface brightness fluctuation have been reanalyzed (J. Tonry, 1996 private communication). This reanalysis suggests that some small changes in the SBF distances for the training set SN Ia's may be appropriate. The only significant change may be in the distance to SN 1992A in NGC 1380. We have tested the effect of removing SN 1992A from the training set. The result is that the independent sample has a dispersion using MLCS of 0.15 mag, $H_0 = 63$ km s^{-1} Mpc^{-1}, and there are no significant changes in our conclusions. Similarly, we have tested the effect of removing all SBF distances from the training set and replacing them, when available, by distances from planetary nebulae luminosity functions. The result is a dispersion using MLCS of 0.15 mag, $H_0 = 64$ km s^{-1} Mpc^{-1}, and again no significant changes in our conclusions.

Richmond et al. (1995) have discussed a conspicious inconsistency with a preliminary SBF distance to NGC 4526 (J. Tonry, 1994 private communication) and the distance from the shape of the SN 1994D light curve. The difference of 0.7 mag for the SBF and supernovae distance moduli to NGC 4526 implies a "greater than 3 σ" mutual rejection. The case can be simplified by comparing the results for SN 1992A in NGC 1380 in Fornax to SN 1994D. These supernovae have identically shaped light curves that, according to a light curve shape–luminosity relation, implies that they have the same luminosity. The preliminary SBF distance to SN 1994D suggests that it was brighter than SN 1992A by 0.5 mag. Such a difference in luminosity between SN Ia's with similar light-curve shapes, if true, must be unusual.

Inclusion of SN 1994D at the preliminary SBF distance has the effect of decreasing the precision of the distance estimates for the independent sample of objects, but the training set is large enough that the effect is not substantial. The dispersion of distances on the Hubble diagram for MLCS increased from 0.12 to 0.22 mag, and the χ^2 increased from 13 to 39. This strong increase in dispersion and χ^2 reinforces our belief that the preliminary SBF distance to NGC 4526 is inconsistent with the distance derived with SN 1994D. Until either another such object is observed or the SBF distance is finalized, we remain agnostic as to which is "correct." We find the MLCS distances to SN 1994D to be 30.83 ± 0.16 and hope that the size and shape of the Virgo Cluster will soon be understood well enough to test this prediction.

In § 5 we developed a formal way to combine our measurement of A_V with our a priori understanding of dust. This method requires some description of the distribution of A_V values for supernovae discovered in galaxies. The most conservative estimate for $p(A_V)$ is that it is constant over the range of equation (22). This amounts to truncation of extinctions less than zero. A Gaussian wing that is a maximum at $A_V = 0.0$ and is parameterized by its second moment seems more plausible. Either assuming a constant value for $p(A_V)$ of a Gaussian wing with $0.5 \leq \sigma \leq \infty$ yields a high level of distance precision. The Hubble diagram dispersion is insensitive to the value of σ over this range, and the Hubble constant is insensitive to any particular parameterization of $p(A_V)$, including requiring $A_V = 0$ (see Table 6). Using a $p(A_V)$ with $\sigma \leq 0.5$ is too restrictive and amounts to discarding any extinction information. Determination of the best value for σ by maximizing the log-likelihood of Equation (15) on the Hubble diagram yields $\sigma = 0.9$ mag. It is important to consider sample selection effects when choosing a form for the observed $p(A_V)$. Clearly the width of $p(A_V)$ could be a function of the search characteristics, since these determine how likely it is to find an SN Ia obscured by dust. Monte Carlo calculations provide an estimate of the effect of misjudging $p(A_V)$, and with enough data, one could solve easily for the distribution of observed A_V.

The MLCS method estimates the total extinction from the supernova line-of-sight reddening. Therefore, we expect this total extinction measure to be equal to or greater than the galactic extinction as derived from the correlation between hydrogen column density and reddening (Burstein & Heiles 1982). Yet, both methods for measuring extinction have uncertainties. For the 20 SN Ia's in our independent sample, 13 have an estimate of MLCS total extinction that equals or exceeds the estimate of galactic extinction (Burstein & Heiles 1982). For the remaining seven SN Ia's, in no case was the MLCS total extinction inconsistent with being equal to the galactic extinction.

Tammann & Sandage (1995) have questioned the validity of our training set distances; "Supernovae used by Phillips (1993)... based on distances determined by the Tully-Fisher and the surface brightness fluctuation methods... clearly deviate from the [Cepheid-calibrated] supernovae values." This criticism is misdirected. While it is true that the *absolute* distance scale as determined by Cepheid variables is not necessarily consistent with the Tully-Fisher and SBF distances, we employ only *relative* distances of these methods to measure the *relative* luminosity variation of SN Ia's out to the Virgo Cluster (Kennicutt et al. 1995). The selection bias pointed out by Sandage (1988a, 1988b, 19994a, 1994b) to distort Tully-Fisher

distances *does not apply* to the distances in our training set that were derived from the bias-corrected inverse Tully-Fisher relation (Strauss & Willick 1995; Schechter 1980; Pierce 1996).

Tammann & Sandage (1995) have also commented on the statistical problem raised by a light curve–luminosity relation stating that "the Malmquist effect on the distant SN Ia's would be overwhelming." Specifically, Tammann & Sandage (1995) argue that the distant SN Ia's occupy "a volume of about 3×10^5 larger, on average, than the volume of the three nearby local calibrators." Therefore, one might expect a substantial selection bias favoring brighter SN Ia's in the distant sample as compared to the SN Ia's nearby. In fact, the mean SN Ia luminosity for the distant sample we use is 0.34 mag *dimmer* than for the set of three nearby calibrators. Is this surprising? Not necessarily. The selection bias, as stated by Tammann & Sandage (1995), assumes a survey that is complete to a limiting magnitude. This is clearly not case for our sample or for theirs. Inspection of the Hubble diagrams of Figure 6 (or of Tammann & Sandage's) does not show the number of SN Ia's increasing with distance as $10^{0.6\mu}$ as expected for a complete search of increasing volume. This point can be made quantitatively by performing a simple $\langle V/V_{\max} \rangle$ test (Schmidt 1968), which has an expectation value of 0.5 for a uniformly distributed sample. For the distant set of 20 SN Ia's $\langle V/V_{\max} \rangle = 0.09$, which shows that this sample is concentrated nearby. Even limiting the test to the set of 12 SN Ia's discovered during the uniform Calán/Tololo survey yields $\langle V/V_{\max} \rangle = 0.16$. Real samples of observed SN Ia's are not distributed as assumed by Tammann & Sandage (1995).

There may be selection parameters other than brightness that influence the discovery of SN Ia's. It has been suggested (N. Suntzeff, 1996 private communication) that at greater distances, photographic surveys, such as the Calán/Tololo survey, may favor the discovery of SN Ia's in elliptical galaxies in which supernovae are easier to discern. It has also been suggested (Branch 1996, Hamuy et al. 1996) that SN Ia's in ellipticals may be intrinsically dimmer than those in later type galaxies. This suggests that at large distances, the sample of SN Ia's may contain a greater proportion of dim objects. Unfortunately, the Hubble diagrams of Figure 6 do not contain enough information to determine whether dim or bright objects are favored at large distances. If we assume naively that there is no selection bias affecting our sample, we find that the chance of the three local calibrators being 0.34 mag dimmer than the independent sample is 6%. This is about as likely as picking randomly the winner of the next baseball American League Championship Series.

An interesting question to consider is what explosion or progenitor parameters could explain our empirically determined variation in light-curve shape, luminosity, and color? Current models have attempted to explain the inhomogeniety of supernovae in one of two ways. Höflich et al. (1995) and Höflich & Khokhlov (1996) have found that a variation in the density at which the deflagration burning front transitions to a detonation wave affects the amount of ^{56}Ni produced in the explosion. A late transition gives the outer layers time to preexpand, resulting in a small nickel production. The reduced nickel heating diminishes the temperatures in the expanding envelope and photosphere. This results in rapidly dropping opacities. Consequently, the photosphere recedes fast and the stored energy is emitted over a short period of time. Conversely, an early turnover of the deflagration into a detonation front results in a large amount of nickel, which produces a bright and hot supernova whose opaque layers keep the radiative energy loss comparably low. This mechanism works for deflagrations, delayed detonations, and pulsating delayed detonations. Qualitatively, the observed correlation between luminosity and the photometric parameters are reproduced (Höflich & Khokhlov 1996).

Another theoretical approach to matching the observations involves exploding progenitors of varying and generally sub-Chandrasekhar mass. A layer of helium accumulates at the base of the static hydrogen-burning zone. Sudden burning of this helium at the base of the layer sends a shock that can trigger a carbon detonation at the interface. If this does not occur, a second chance at carbon detonation can come when the shock propagates around the star and converges on the opposite site. The variation in progenitor mass suggests a simpler connection to the amount of nickel produced than the Chandrasekhar models. Again the variation in nickel yield is expected to match the observed correlations in supernova observables. These models have been successful in one and two dimensions, but it remains to be seen if the abundance and the velocity distribution of the intermediate-mass elements produced from nucleosynthesis matches the observations (Livne & Arnett 1995; Woosley & Weaver 1994; Livne 1990; Livne & Glasner 1990).

Finally, improvements can be made in the MLCS technique when we acquire a larger training set of supernovae. First, the "gray snakes" of Figure 3 and the relative weights of the B, V, R, and I data determined from equation (16) suggest that greater precision could be attained by including a quadratic term in the light-curve shapes model for B-, R-, and I-band data. An additional order in the fit would demand a larger training set of data to avoid overfitting the details of the training set objects. A larger training set would also support the determination of a more detailed correlation matrix with estimates of model residual covariances.

The MLCS technique provides an exceedingly precise way of measuring extinction-corrected distances with uncertainty estimates. The redshifts to which Type Ia supernova light curves can measure distances have interesting implications for cosmological measurements. Two teams are currently laboring to find and measure SN Ia's at $0.3 \leq z \leq 0.6$ (Perlmutter et al. 1996; Schmidt et al. 1996) with the intent of measuring the cosmological deceleration of the universe, q_0. At these redshifts, SN Ia light curves are difficult to obtain, and informative spectra are even harder, so it is sensible to use all the available SN Ia's. The uncertainty in q_0 is proportional to the distance precision divided by the square root of the number of objects. The MLCS method should help with both these factors by including all well-observed SN Ia's in the sample and increasing the precision of SN Ia distance measures.

We are again grateful to Mario Hamuy, Mark Phillips, Nick Suntzeff, and the entire Calán/Tololo collaboration for the opportunity to study their exceptional data before publication. We have benefited greatly from discussions with Brian Schmidt, George Rybicki, and Peter Höflich. This work was supported through NSF grants AST 92-18475 and PHY 95-07695.

REFERENCES

Arnett, W. D. 1969, Ap&SS, 5, 280
Arnett, W. D., Branch, D., & Wheeler, J. C. 1985, Nature, 314, 337
Baade, W. 1938, A0J, 88, 285
Baade, W., & Zwicky, F. 1934, Proc. Natl. Acad. Sci., 20, 254
Barbon, R., Ciatti, F., & Rosino, L. 1973, A&A, 25, 65
Boisseau, J. R., & Wheeler, J. C. 1991, AJ, 101, 1281
Branch, D. 1992, ApJ, 392, 35
———. 1996, private communication
Branch, D., Fisher, A., & Nugent, P. 1993, AJ, 106, 2383
Branch, D., & Miller, D. 1993, ApJ, 405, L5
Branch, D., & Tammann, G. A. 1992, ARA&A, 30, 359
Burstein, D., & Heiles, C. 1982, AJ, 87, 1165
Buta, R. J., & Turner, A. 1983, PASP, 95, 72
Capaccioli, M., Cappellaro, E., Della Valle, M., D'Onofrio, M., Rosino, L., & Turatto, M. 1990, ApJ, 350, 110
Chapman, G. 1988, AJ, 95, 999
Ciardullo, R., Jacoby, G. H., & Tonry, J. L. 1993, ApJ, 419, 479
Colgate, S., & McKee, W. 1969, ApJ, 157, 623
Cristiani, S., et al. 1992, A&A, 259, 63
Curtis, H. D. 1921, BNRCNAS, 2, 171
Davis, M., & Peebles, P. J. E. 1983, ApJ, 267, 465
de Vaucouleurs, G., et al. 1991, Third Reference Catalogue of Bright Galaxies (New York: Springer)
Dell'Antonio, I. 1995, private communication
Della Valle, M., & Panagia, N. 1992, AJ, 104, 696
Doggett, J. B., & Branch, D. 1985, AJ, 90, 2303
Feast, M. W., & Walker, A. R. 1987, ARA&A, 25, 345
Filippenko, A. V., et al. 1992, AJ, 104, 1543
———. 1996, in preparation
Ford, C., et al. 1993, AJ, 106, 3
Goldhaber, G., et al. 1996, in preparation
Hamuy, M., Phillips, M. M., Maza, J., Suntzeff, N. B., Schommer, R. A., & Aviles, A. 1994, AJ, 108, 2226
———. 1995, AJ, 109, 1
———. 1996, in preparation
Hamuy, M., Phillips, M., Wells, L., & Maza, J. 1993b, PASP, 105, 787
Hamuy, M., et al. 1991, AJ, 102, 208
———. 1993a, AJ, 106, 2392
Hoyle, F., & Fowler, W. A. 1960, ApJ, 132, 565
Höflich, P., & Khokhlov, A. 1996, ApJ, 457, 500
Höflich, P., Müller, E., & Khokhlov, A. 1993, A&A, 268, 570
Höflich, P., Khokhlov, A., & Wheeler, J. C. 1995, ApJ, 444, 831
Humason, M. L., Mayall, N. U., & Sandage, A. R. 1956, AJ, 61, 97
Jacoby, G. H., et al. 1992, PASP, 104, 678
Jerjen, H., & Tammann, G. A. 1993, A&A, 276, 1
Joëever, M. 1982, Astrofizica, 18, 574
Kennicutt, R. C., Freedman, W. L., & Mould, J. R. 1995, AJ, 110, 1476
Khokhlov, A., Müller, E., & Höflich, P. 1993, A&A, 270, 223
Kirshner, R. P., Oke, J. B., Penston, M. V., & Searle, L. 1973, ApJ, 185, 303
Kowal, C. T. 1968, AJ, 73, 1021
Lauer, T. R., & Postman, M. 1992, ApJ, 400, L47
———. 1994, ApJ, 425, 418
Leibundgut, B. 1989, Ph.D. thesis, Basel
Leibundgut, B., et al. 1991, ApJ, 371, L23
———. 1993, AJ, 105, 301
———. 1996, ApJ, submitted
Lira, P. 1995, Masters thesis, Univ. Chile
Livne, E. 1990, ApJ, 354, L53
Livne, E., & Arnett, D. 1995, ApJ, 452, 62
Livne, E., & Glasner, A. S. 1990, ApJ, 361, L244
Lynden-Bell, D., & Lahav, O. 1988, in Large-Scale Motions in the Universe, ed. V. C. Rubin & G. V. Coyle (Princeton: Princeton Univ. Press), 199
Marzke, R. O., Geller, M. J., da Costa, L. N., & Huchra, J. P. 1995, AJ, 110, 477
Maza, J., Humuy, M., Phillips, M., Suntzeff, N., & Aviles, R. 1994, ApJ, 424, L107
Mazurek, T. J., & Wheeler, J. C. 1980, Fundam. Cosmic Phys., 5, 193
Miller, D., & Branch, D. 1990, AJ, 100, 530
Minkowski, R. 1941, PASP, 53, 224
———. 1964, ARA&A, 2, 247
Nomoto, K., Thielemann, F., & Yokoi, K. 1984, ApJ, 286, 644
Oke, J. B., & Sandage, A. 1968, ApJ, 154, 21
Oke, J. B., & Searle, L. 1974, AR&A, 12, 315
Perlmutter, S., et al. 1995, ApJ, 440, 41
———. 1996, NASI, Aiquablava, Spain, in preparation
Phillips, M. 1993, ApJ, L105
Phillips, M., Wells, L., Suntzeff, N., Hamuy M., Leibundgut, B., Kirshner, R. P., & Foltz, C. 1992, AJ, 103, 1632
Phillips, M., et al. 1987, PASP, 99, 592
Pierce, M. J. 1994, ApJ, 430, 53
———. 1996, BAAS, 27, 4
Press, W. H., Teukolsky, S. A., Vetterling, W. T., & Flannery, B. P. 1992, Numerical Recipes (2d ed.; Cambridge University Press)
Pskovskii, Y. 1977, Soviet Astron., 21, 675
———.1984, Soviet Astron., 28, 658
Richmond, M. W., Treffers, R. R., Filippenko, A. V., Van Dyk, S. D., Paik, Y., & Peng, C. 1995, AJ, 109, 2121
Riess, A. G., Press, W. H., & Kirshner, R. P. 1995a, ApJ, 438, L17 (RPK95a)
———. 1995b, ApJ, 445, L91
———. 1996b, in preparation
Riess, A. G., et al. 1996a, in preparation
Rood, H. J. 1994, PASP, 106, 170
Ruiz-Lapuente, P., et al. 1993, Nature, 365, 728
Rybicki, G., & Kleyna, J. T. 1994, in Reverberation Mapping of the Broad-Line Region in Active Galactic Nuclei, ed. P. M. Gondhalekar, K. Horne, & B. M. Peterson (San Francisco: ASP), 85
Rybicki, G., & Press, W. 1992, ApJ, 398, 169
Sandage, A. 1988a, ApJ, 331, 583
———. 1988b, ApJ, 331, 605
———. 1994a, ApJ, 430, 1
———. 1994b, ApJ, 430, 13
Sandage, A., & Tammann, G. A. 1993, ApJ, 415, 1
Sandage, A., Tammann, G. A., Panagia, N., & Macchetto, D. 1992, ApJ, 401, 7L
Sandage, A., et al. 1994, ApJ, 423, L13
———. 1996, ApJ, in press
Savage, B. D., & Mathis, J. S. 1979, ARA&A, 17, 73
Schaefer, B. E. 1994, ApJ, 426, 493
———. 1995a, ApJ, 447, L13
———. 1995b, ApJ, 449, L9
———. 1996, in preparation
Schecter, P. L. 1980, AJ, 85, 801
Schmidt, B. P., Kirshner, R. P., & Eastman, R. 1992, ApJ, 395, 366
Schmidt, B. P., et al. 1996, in preparation
Schmidt, M. 1968, ApJ, 151, 393
Shapley, H. 1921, BNRCNAS, 2, 171
Smoot, G. F., et al. 1992, ApJ, 396, L1
Strauss, M. A., & Willick, J. A. 1995, Phys. Rev. 1995, 261, 271
Suntzeff, N. B. 1993, in IAU Colloq. 145, Supernovae and Supernovae Remnants, ed. R. McCray (Cambridge: Cambridge Univ. Press), 100
Suntzeff, N. B., et al. 1996, in preparation
Tammann, G. A. 1987, in IAU Symp. 124, Observational Cosmology, ed. A. Hewitt, G. Burbidge, & L. Z. Fang (Dordrecht: Reidel), 151
Tammann, G. A., & Leibundgut, B. 1990, A&A, 236, 9
Tammann, G. A., & Sandage, A. 1995, ApJ, 452, 16
Tonry, J. L. 1991, ApJ, 373, L1
Uomoto, A., & Kirshner, R. P. 1985, A&A, 149, L7
van den Bergh, S. 1995, ApJ, 453, L55
Vaughan, T. E., Branch, D., Miller, D. L., & Perlmutter, S. 1995, ApJ, 439, 558
Wells, L. A., et al. 1994, AJ, 108, 2233
Wheeler, J. C., & Levreault, R. 1985, ApJ, 294, L17
Wheeler, J. C., & Harkness, R. P. 1990, Rep. Prog. Phys., 53, 1467
Woosley, S. E., & Weaver, T. A. 1994, ApJ, 423, 371